BIOPHYSICAL JOURNAL

published bimonthly for the Biophysical Society

by The Rockefeller Institute Press

Editorial Board

THOMAS F. ANDERSON
FRANK BRINK, JR. *Editor*
KENNETH S. COLE
ARNE ENGSTROM
JAMES D. HARDY
JOHN C. KENDREW
MAX A. LAUFFER, JR.
LAWRENCE J. ONCLEY
HENRY QUASTLER
EUGENE I. RABINOWITCH
ALEXANDER RICH
RICHARD B. ROBERTS
WALTER A. ROSENBLITH
CORNELIUS A. TOBIAS
ROBLEY WILLIAMS
RAYMOND E. ZIRKLE

VOLUME 1 NEW YORK 1961

Copyright, 1961, by The Rockefeller Institute Press

CONTENTS

NUMBER 1, SEPTEMBER, 1960

POTASSIUM ION CURRENT IN THE SQUID GIANT AXON: DYNAMIC CHARACTERISTIC. *Kenneth S. Cole and John W. Moore* 1

AN APPROACH TO THE QUANTITATIVE ANALYSIS OF ELECTROPHYSIOLOGICAL DATA FROM SINGLE NEURONS. *George L. Gerstein and Nelson Y.-S. Kiang* 15

THE ULTRAVIOLET LIGHT INACTIVATION OF ΦX174 BACTERIOPHAGE AT DIFFERENT WAVE LENGTHS AND pH's. *R. B. Setlow and Richard Boyce* 29

PHYSICAL STUDIES ON POX VIRUSES. I. INACTIVATION OF VACCINIA VIRUS INFECTIVITY WITH LOW-ENERGY ELECTRONS. *J. F. McCrea, John W. Preiss, and Jean O'Loughlin* 43

THE STRUCTURE OF TOBACCO MOSAIC VIRUS AND ITS COMPONENTS: ULTRAVIOLET OPTICAL ROTATORY DISPERSION. *Norman S. Simmons and Elkan R. Blout* 55

CHANGES IN QUANTUM YIELD OF PHOTOSYNTHESIS IN THE RED ALGA *Porphyridium cruentum* CAUSED BY STEPWISE REDUCTION IN THE INTENSITY OF LIGHT PREFERENTIALLY ABSORBED BY THE PHYCOBILINS. *Jan B. Thomas and Govindjee* 63

NUMBER 2, NOVEMBER, 1960

ACTION SPECTRUM OF THE "SECOND EMERSON EFFECT." *Govindjee and Eugene Rabinowitch* 73

INHIBITION OF PHOTOSYNTHESIS IN CERTAIN ALGAE BY EXTREME RED LIGHT. *Govindjee, Eugene Rabinowitch, and Jan B. Thomas* 91

THE PHOTOCONDUCTIVITY OF CHLOROPLASTS AND THE FAR RED LIGHT EFFECT. *Shoji Ichimura* 99

THE KINETICS OF DISTRIBUTION OF THE FAT-SOLUBLE INERT GAS CYCLOPROPANE IN THE BODY. *W. Perl, G. T. Lesser, and J. M. Steele* 111

MICROEXUDATES FROM CELLS GROWN IN TISSUE CULTURE. *Murray D. Rosenberg* 137

ANALYSIS OF CERTAIN ERRORS IN SQUID AXON VOLTAGE CLAMP MEASUREMENTS. *Robert E. Taylor, John W. Moore, and Kenneth S. Cole* 161

LETTERS TO THE EDITOR 203

NUMBER 3, JANUARY, 1961

THEORY OF DIFFUSION IN GELS. *Max A. Lauffer* 205

STUDIES OF *E. coli* RIBOSOMAL RNA AND ITS DEGRADATION PRODUCTS. *Arthur I. Aronson and Brian J. McCarthy* 215

THE KINETICS OF THE SYNTHESIS OF RIBOSOMAL RNA IN *E. coli*. *Brian J. McCarthy and Arthur I. Aronson* 227

PHYSICAL AND TEMPORAL FACTORS INVOLVED IN THE DEATH OF YEAST AT SUBZERO TEMPERATURES. *Peter Mazur* 247

206829

NUMBER 4, MARCH, 1961

RADIATION INHIBITION OF AMINO ACID UPTAKE BY *Escherichia coli*. *E. S. Kempner and Ernest C. Pollard* 265

DYNAMIC CHARACTERISTICS OF THE MOTOR COORDINATION SYSTEM IN MAN. *Lawrence Stark, Mitsuo Iida, and Paul A. Willis* 279

THE MOLECULAR WEIGHT AND AGGREGATION OF DNA. *Liebe F. Cavalieri, Joan F. Deutsch, and Barbara Hatch Rosenberg* 301

THE REPLICATION OF DNA. I. TWO MOLECULAR CLASSES OF DNA. *Liebe F. Cavalieri and Barbara Hatch Rosenberg* 317

THE REPLICATION OF DNA. II. THE NUMBER OF POLYNUCLEOTIDE STRANDS IN THE CONSERVED UNIT OF DNA. *Liebe F. Cavalieri and Barbara Hatch Rosenberg* 323

THE REPLICATION OF DNA. III. CHANGES IN THE NUMBER OF STRANDS IN *E. coli* DNA DURING ITS REPLICATION CYCLE. *Liebe F. Cavalieri and Barbara Hatch Rosenberg* 337

ANOMALOUS IMPEDANCE, A PHENOMENOLOGICAL PROPERTY OF TIME-VARIANT RESISTANCE. AN ANALYTIC REVIEW. *Alexander Mauro* 353

LETTERS TO THE EDITOR 373

NUMBER 5, MAY, 1961

STUDIES ON THE SECOND EMERSON EFFECT IN THE HILL REACTION IN ALGAL CELLS. *Rajni Govindjee and Eugene Rabinowitch* 377

DAMAGE BY VISIBLE LIGHT TO THE ACRIDINE ORANGE–DNA COMPLEX. *David Freifelder, Peter F. Davison, and E. Peter Geiduschek* 389

AN ANALYSIS OF THE MEMBRANE POTENTIAL ALONG A CLAMPED SQUID AXON. *Kenneth S. Cole* 401

ENERGY EXPENDITURE BY ACTIVE TRANSPORT MECHANISMS. II. FURTHER GENERALIZATIONS. *Clifford S. Patlak* 419

LOCALIZATION OF β-GALACTOSIDASE IN CELLS OF *Escherichia coli* BY LOW VOLTAGE ELECTRON BOMBARDMENT. *John W. Preiss and Ernest C. Pollard* 429

NUMBER 6, JULY, 1961

IMMUNOENZYMOLOGICAL EVIDENCE SUGGESTING A CHANGE IN CONFORMATION OF ADENYLIC ACID DEAMINASE AND CREATINE KINASE DURING SUBSTRATE COMBINATION. *Arthur J. Samuels* 437

IMPULSES AND PHYSIOLOGICAL STATES IN THEORETICAL MODELS OF NERVE MEMBRANE. *Richard FitzHugh* 445

STUDIES ON THE STRUCTURE OF FEATHER KERATIN. I. X-RAY DIFFRACTION STUDIES AND OTHER EXPERIMENTAL DATA. *R. Schor and S. Krimm* 467

STUDIES ON THE STRUCTURE OF FEATHER KERATIN. II. A β-HELIX MODEL FOR THE STRUCTURE OF FEATHER KERATIN. *R. Schor and S. Krimm* 489

A COMPARISON OF THE NATIVE AND DERIVED 30S AND 50S RIBOSOMES OF *Escherichia coli*. *Melvin H. Green and Benjamin D. Hall* 517

NUMBER 7, SEPTEMBER, 1961

THE STRUCTURE OF HIGH MOLECULAR WEIGHT RIBONUCLEIC ACID IN SOLUTION. A SMALL-ANGLE X-RAY SCATTERING STUDY. *Serge N. Timasheff, J. Witz, and V. Luzzati* 525

THE LONG WAVE LENGTH FORMS OF CHLOROPHYLL *a*. *Jeanette S. Brown and C. Stacy French* 539

REVERSAL OF PHOTORECEPTOR POLARITY RECORDED DURING THE GRADED RECEPTOR POTENTIAL RESPONSE TO LIGHT IN THE EYE OF *Limulus*. *R. M. Benolken* 551

THE PHYSICS OF BLOOD FLOW IN CAPILLARIES. I. THE NATURE OF THE MOTION. *J. Prothero and A. C. Burton* 565

A PROPERTY OF SECOND ORDER DIFFERENTIAL EQUATIONS WITH APPLICATION TO FORMAL KINETICS. *John Z. Hearon* 581

QUANTITATIVE RADIOAUTOGRAPHIC STUDIES ON EXPONENTIALLY GROWING CULTURES OF *Escherichia coli*. THE DISTRIBUTION OF PARENTAL DNA, RNA, PROTEIN, AND CELL WALL AMONG PROGENY CELLS. *R. P. Van Tubergen and Richard B. Setlow* 589

NUMBER 8, NOVEMBER, 1961

EFFECTS OF THE VESSEL WALL ON ELECTROMAGNETIC FLOW MEASUREMENT. *Urs Gessner* 627

KINETIC STUDIES OF β-GALACTOSIDASE INDUCTION. *J. A. Boezi and Dean B. Cowie* 639

A MODEL FOR THE MECHANISM OF ENZYME INDUCTION. *R. B. Roberts, R. J. Britten, and F. T. McClure* 649

AN X-RAY SCATTERING INVESTIGATION OF WILD CUCUMBER MOSAIC VIRUS AND A RELATED PROTEIN. *J. W. Anderegg, P. H. Geil, W. W. Beeman, and Paul Kaesberg* 657

COMPUTER SOLUTIONS FOR PHOTOSYNTHESIS RATES FROM A TWO PIGMENT MODEL. *C. S. French and D. C. Fork* 669

ON THE ORIGIN OF MACROMOLECULAR SEQUENCES. *Howard H. Pattee* 683

SPECTROSCOPIC EVIDENCE FOR COMPLEXING OF ACETIC ACID WITH BOVINE SERUM ALBUMIN, GRAMICIDIN, AND DIMETHYLFORMAMIDE. *John R. Cann* 711

LETTERS TO THE EDITOR 723

INDEX TO VOLUME 1 727

POTASSIUM ION CURRENT IN THE SQUID GIANT AXON: DYNAMIC CHARACTERISTIC

KENNETH S. COLE *and* JOHN W. MOORE

From the National Institutes of Health, Bethesda, Maryland, and the Marine Biological Laboratory, Woods Hole, Massachusetts

ABSTRACT Measurements of the potassium current in the squid axon membrane have been made, after changes of the membrane potential to the sodium potential of Hodgkin and Huxley (HH), from near the resting potential, from depolarizations of various durations and amplitudes, and from hyperpolarizations of up to 150 mv. The potassium currents I given by

$$I = I_\infty\{1 - \exp[-(t + t_0)/\tau]\}^{25},$$

where t_0 is determined by the initial conditions, represent the new data and approximate the HH functions in the regions for which they are adequate. A corresponding modification for the sodium current does not appear necessary. The results support the HH assumptions of the independence of the potassium and sodium currents, the dependence of the potassium current upon a single parameter determined by the membrane potential, and the expression of this parameter by a first order differential equation, and, although the results drastically modify the analytical expressions, they very considerably extend the range of apparent validity of these assumptions. The delay in the potassium current after severe hyperpolarization is used to estimate a potassium ion mobility in the membrane as 10^{-5} of its value in aqueous solutions.

Hodgkin and Huxley, (HH I)[1] have separated the current flow across the squid axon membrane, after a change of the membrane potential, into two principal components, a sodium ion current, I_{Na}, and a potassium ion current, I_K. Each of these currents was expressed (HH II) in terms of the respective conductances g_{Na} and g_K, and the membrane potentials at which the respective currents were zero, the sodium and potassium potential E_{Na} and E_K. The total current is

$$I = I_{Na} + I_K = g_{Na}(V - E_{Na}) + g_K(V - E_K),$$

where V is the membrane potential difference and the leakage current I_L is ignored for the present.

A preliminary report has been made (Cole, 1958).
Received for publication, March 31, 1960.

[1] Hodgkin and Huxley will be referred to by HH and their four papers 1952*a*, *b*, *c*, *d* by I, II, III, IV.

As a part of our program to make a critical survey and evaluation of the HH formulations of the properties of the squid giant axon membrane, we have investigated the time course of the potassium ion current I_K. Instead of following the extensive HH experimental and analytical procedures based on choline substitution for external sodium, we have restricted ourselves to measurements made at or near the sodium potential. At $V = E_{Na}$, $I_{Na} = 0$, and $I = I_K = g_K (V - E_K)$ no matter what the value of g_{Na}.

Hodgkin and Huxley (HH IV) expressed their potassium conductance data by $g_K = \bar{g}_K n^4$ where $\bar{g}_K$ is a constant and n is a parameter, something like a probability, varying from zero to unity and given by the differential equation

$$dn/dt = (n_\infty - n)/\tau \tag{1}$$

n_∞ and τ are defined empirically as functions of the membrane potential with n_∞ as the steady state value and τ as a time constant of the approach to that value.

If at $t = 0$, $n = n_0$ and for $t > 0$, $V = E_{Na}$ then $n = n_\infty - (n_\infty - n_0) \exp(-t/\tau)$ is the appropriate solution of equation (1) with n_∞ as the steady state value. When $n_0 = 0$

$$\begin{aligned} I &= \bar{g}_K n_\infty^4 [1 - \exp(-t/\tau)]^4 (V - E_K) \\ &= I_\infty [1 - \exp(-t/\tau)]^4 \end{aligned} \tag{2}.$$

For $0 < n_0 < 1$,

$$\begin{aligned} n &= n_\infty \left[1 - \frac{n_\infty - n_0}{n_\infty} \exp(-t/\tau) \right] \\ &= n_\infty [1 - \exp(-t_0/\tau) \exp(-t/\tau)] \\ &= n_\infty \{1 - \exp[-(t + t_0)/\tau]\} \end{aligned} \tag{3},$$

where $t_0 = \tau \ln[n_\infty/(n_\infty - n_0)]$

is the time in which n would have risen from zero to the initial value of n_0 at $t = 0$. The initial condition, n_0, is usually unimportant for an equivalent delay of $t_0 < 0.1\ \tau$ and certainly so for $t_0 < 0.01\ \tau$. The corresponding values of n_0, which the HH axon reaches for hyperpolarizations of less than 20 and 50 mv, are then $n_0 < 0.1\ n_\infty$ and $n_0 < 0.01\ n_\infty$ respectively.

The experimental work has been done in three phases. In the first I has been measured after a step change of the membrane potential from near the resting potential to the sodium potential and compared with equation (2) for several environmental conditions. In the second phase, the step to E_{Na} was made after initial depolarizations of various amplitudes and durations. I was compared with equation (3), as suggested by Dr. Richard FitzHugh, to test the assumption that it was the function of the single parameter, n, described by a first order differential equation. The third phase was an extension of the second, in which continuous or comparatively long hyperpolarization was applied to the membrane before the test steps to E_{Na}. Some observations on the effect of initial hyperpolarization on the ion cur-

rents during potential steps to other than the sodium potential are included as a fourth phase.

The results of the first two phases are much as had been anticipated. Those of the third phase require such a considerable modification and extension of the HH formulation that it becomes essentially a new expression for the potassium current. The need of a similar alteration for the sodium current is not apparent.

EXPERIMENTAL

The giant axon in the hindmost stellar nerve of the squid, *Loligo pealii*, has been used throughout as shown schematically in Fig. 1 and discussed and described in detail by Cole and Moore (1960) and Moore and Cole (1961). The membrane potential is measured

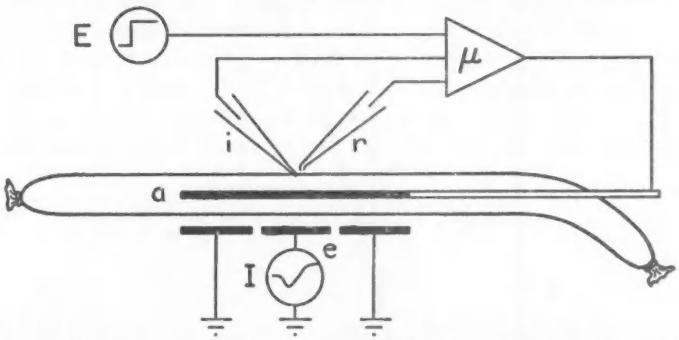

FIGURE 1 Diagram of method for control of the membrane potential. The potential is measured between the micropipette, internal, and capillary, external, electrodes, *i* and *r*. The electronic control system, μ, provides the current between the internal axial and external electrodes, *a* and *e*, needed for the membrane potential to follow the command potential, *E*. The membrane current, *I*, is measured for a length of axon corresponding to the guarded central electrode, *e*. (Reproduced from Moore, 1959*b*, with permission.)

between the micropipette internal and capillary external potential electrodes, *i* and *r*, and controlled by the electronic system μ. This system applies such a potential to the internal axial wire, *a*, as is necessary to force the membrane potential to follow the command potential, *E*, within tens of microseconds and a few millivolts. The membrane potential is usually held at a constant value somewhat more negative than the resting potential and the experimental steps are applied from this holding potential E_H. The membrane current, *I*, is measured over the length of axon determined by the central, guarded, external electrode, *e*.

RESULTS

1. *Initial Resting Potential.* The records of this first phase were made in 1956 with the assistance of Professor Ulrich Franck and subsequently mostly measured and analyzed by him. The four axons were held hyperpolarized by several

millivolts from the resting potentials and steps were applied to bring the potential to that value, E_{Na}, at which no initial sodium current was seen. Twenty-seven current records were made at sodium potentials which were varied from 0 to +50 mv, at temperatures from 5°C to 20°C, and with a few changes of external Ca and K concentrations. The initial current was subtracted and the steady state current, I_∞, was extrapolated to approximately correct for any slow "droop" after the maximum. These data, I, from individual records were plotted as log I *versus* log t and superposed as shown in Fig. 2.

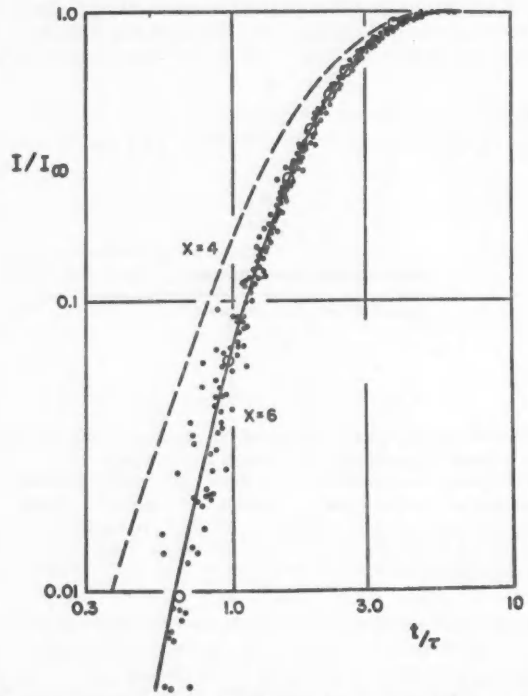

FIGURE 2 Potassium current, I, as a function of time, t, after changes from near resting to the sodium potential, with I_∞ as the steady state current and τ the time constant of the process. The points are from four 1956 axons and the circles are from HH IV, Fig. 3. The solid line is given by equation (4) and the broken line by equation (2).

The data of Fig. 2 are rather well represented by the solid curve

$$I = I_\infty[1 - \exp(-t/\tau)]^6 \qquad (4)$$

but it was often necessary to take the origin for time to be somewhat different from that at which the potential was actually changed. Thus these data have been fitted

by an equation, such as equation (3), involving t_0, and so depending upon the initial condition, n_0. The variations of n_0 are attributed to differences between the axons and the holding potentials, E_H, used for them.

As HH suggested might be the case and is illustrated by points from their data on Fig. 2, this higher power of the time function is clearly more satisfactory than the broken line which is the fourth power they found more convenient to use. We see no basis to disagree with the HH conclusion that the difference between the exponents of 6 and 4 is not particularly important, so this phase is essentially a confirmation of their analysis.

2. *Initial Depolarization.* Potential steps to E_{Na} were made in this second phase either at successive times after the start of preliminary depolarizing steps or at fixed times after the start of preliminary steps having various amplitudes. Examples of the membrane current patterns for both procedures are shown in Figs. 3*a* and 4*a* and the corresponding superpositions of the currents at E_{Na} by translations on the time axis are given as Figs. 3*b* and 4*b*. These superpositions are quite good except for the capacity transients and the early excess outward currents. The latter were often smaller than those in Figs. 3*b* and 4*b* but were also sometimes larger.

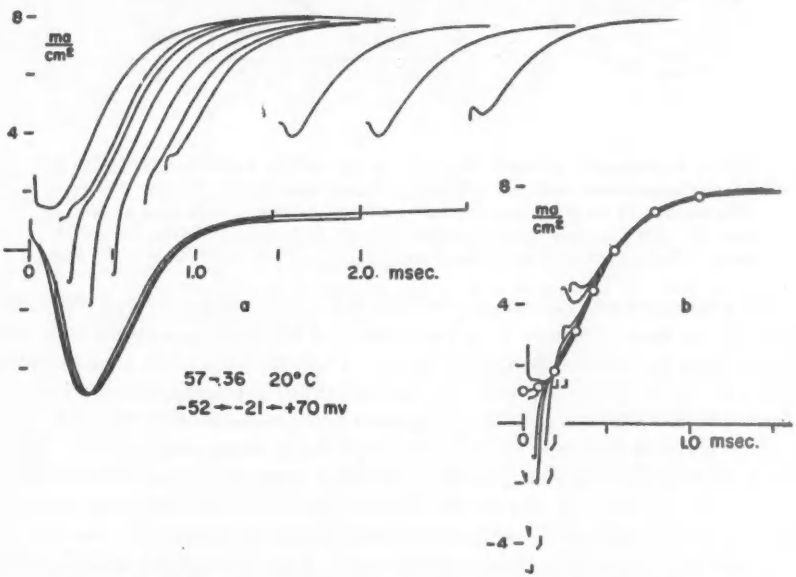

FIGURE 3*a* Potassium currents obtained at 70 mv, after various durations of an initial depolarization to −21 mv from a holding potential of −52 mv. FIGURE 3*b* Superposition of the potassium currents by changes of origin of time scale as in equation (3). The times and currents at the ends of the initial depolarizations are also shown. Circles are computed by equation (6) for $t_0 = 0.29$ msec. and $\tau = 0.2$ msec.

A small hyperpolarization was routinely used for E_H in these experiments and the end of the capacity transient, a small sodium current, and the beginning of the potassium current often overlapped. This led to the choice of a value for the sodium potential which was afterwards found to be somewhat too high. These sodium currents are quite clear and constant at the beginning of the three slowest test step responses of Fig. 4*a*. Their increase and decrease with increasing initial depolarizations, as seen in Fig. 4*b*, is much as is to be expected from the corresponding changes of the sodium conductance g_{Na}.

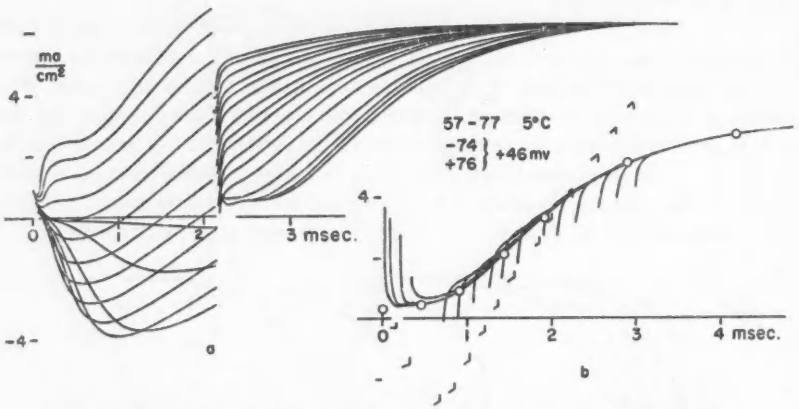

FIGURE 4*a* Potassium currents obtained near the sodium potential after initial depolarizations between −74 and +76 mv in 10 mv steps. $E_H = -74$ mv. FIGURE 4*b* Superposition of the potassium currents by change of origin of time scale as in equation (3). The times and currents at the ends of the initial depolarizations are also shown. Circles are computed by equation (6) for $t_0 = 1.3$ msec. and $\tau = 0.9$ msec.

Except for this early current, the currents at E_{Na} have also superposed very satisfactorily for many combinations of initial potential and duration, external ions, and temperature and indicate the general validity of an expression of the form of equation (3). In the course of these experiments, the initial potential has been varied from −50 to +100 mv, and the sodium parameters, m and h (HH IV), from near zero to one, and from near unity to zero respectively, without any apparent effect upon the standard time course of the potassium current as displaced because of its own initial condition. Furthermore these data are consistent with those near the resting potential and agree as well as the later with the HH formulation.

These initial depolarization experiments are in good agreement with the basic HH assumption that the potassium current is a function of a single variable, such as n. Although the evidence is not clean cut, the explanation of the anomalies seems both reasonable and probable.

3. *Initial Hyperpolarization.* The initial hyperpolarizations were first ap-

plied continuously between the test steps to E_{Na} and later as prepulses of a few milliseconds duration. They were varied up to —210 or —150 mv relative to the resting potentials in the neighborhood of —60 mv. Occasionally the current necessary to maintain the highest hyperpolarization would increase until a membrane breakdown or the removal of the potential.

A typical series of membrane current records is shown in Fig. 5*a* for 3 msec. prepulse potentials up to —212 mv. The initial capacity transients increase regularly but merge into a slower component, after the hyperpolarizations at —162 and

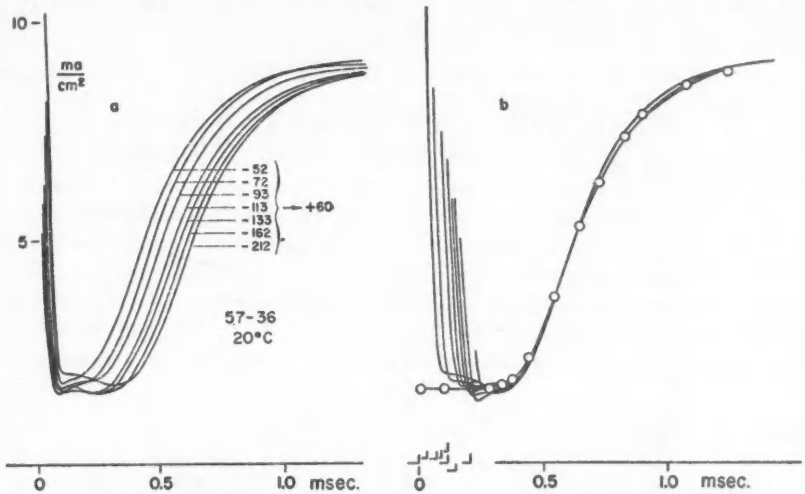

FIGURE 5*a* Potassium currents obtained near the sodium potential after 3 msec. hyperpolarizations at the indicated potentials. FIGURE 5*b* Superposition of the potassium currents by change of origin of time scale as in equation (3). The ends of the initial hyperpolarizations are also shown. Circles are computed by equation (5) for $\tau = 0.18$ msec.

—212 mv, that may be an indication of an incipient membrane breakdown. The initial sodium currents here appear even more clearly than in Figs. 3*a* and 4*a* because of the delayed onset of *I*. It is to be noticed that the delay, shape, and amplitude of this sodium current are not obviously and consistently affected by the amplitude of the hyperpolarization preceding the pulse.

As was done for the initial depolarizations, the current curves of Fig. 5*a* have been superposed by translations along the time axis as shown in Fig. 5*b*. Here the coincidence is better than in the previous examples probably because the interference of the sodium transient is not so confusing. Consequently these currents also can be expressed as a function of $t_0 + t$ where t_0 is again some function of the initial hyperpolarization. The currents are, however, delayed far too much to allow

the use of the HH fourth power function or even the sixth power as found above. To the extent that equation (4) is considered an adequate expression of the potassium current after a step change from near the resting potential to the sodium potential, the assumption that $n_0 = 0$ might be justified. But if this is true there should be no further change of n_0 or the current curve on hyperpolarization—quite contrary to these experimental findings. Even though the assumption of $n_0 = 0$ near the resting potential is not justified, we may, however, try again and assume that there is no potassium current flow at the maximum hyperpolarization used, so $n_0 = 0$ at $E_H = -212$ mv. It is then found that the potassium current after the step to the sodium potential is given rather well by

$$I = I_\infty[1 - \exp(-t/\tau)]^{25} \tag{5}$$

as shown by the circles on Fig. 5*b* and here again, in spite of the drastic change of the exponent, the results of less hyperpolarization are clearly expressible in the form of equation (3).

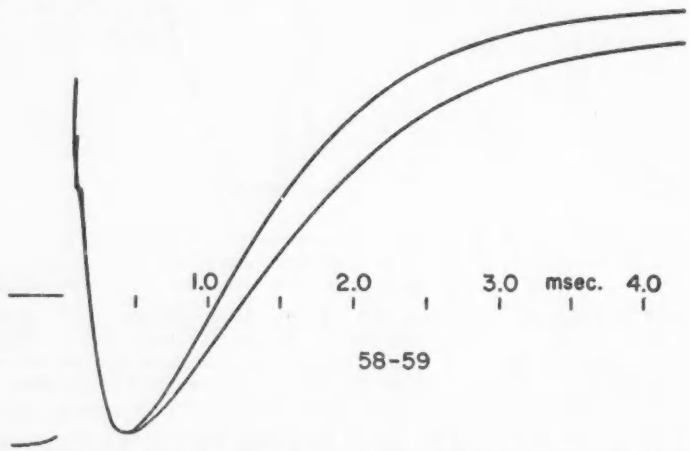

FIGURE 6 Superposition of two ionic currents records at $V = +5$ mv after initial 10 msec. hyperpolarizatons at -75 and -175 mv.

4. The principal phases above have the limitation that they depend upon measurements at rather few values of the sodium potential. It is therefore possible that such observations and conclusions are only valid with little or no sodium current. They can furthermore give but slight indication of the characteristics of the sodium current—particularly as influenced by hyperpolarization.

For other purposes, records have been made of the ionic current at potentials below E_{Na} after various initial hyperpolarizations. The peak inward current attains a maximum, saturation, value, corresponding to $h = 1$ in the HH formulation, for

initial hyperpolarizations at −80 mv or more. Fig. 6 is typical of many other records in showing the superposition after two different initial hyperpolarizations that are both more than the value for inward peak current saturation. The identity of currents up to the time of the inward maximum strongly suggests that the HH sodium "on" process, described by m, is not affected by such initial hyperpolarization and is also indicative of a similar lack of effect on the sodium "off," given by h. However, the delay in current between the inward maximum and the outward steady state after increased initial hyperpolarization is most simply and consistently —if not uniquely—explained as an effect on only the potassium component, just as found at the sodium potential. The fact that such a "shift" does not appear before the maximum is consistent with other indications that, beyond saturation hyperpolarization, the potassium current is not appreciable until after the sodium maximum. It is also observed, in such records as those of Fig. 5*a*, that the small early sodium currents are very similar for all initial hyperpolarizations and are certainly not altered by an amount at all comparable to that found in the later potassium currents. The same appears to be true as seen after the small initial depolarizations of Fig. 4*a*. Both of these types of experiments support at least a tentative conclusion that, above saturation, the sodium currents do not depend upon initial hyperpolarization. Then, with consistent reservations, the delay of potassium current during the sodium "off" process is evidence that this delay can take place in the presence of a sodium current—although the quantitative details have not been investigated.

DISCUSSION

It now becomes quite evident that the regularity of the early results, given in the first phase, is probably most significant as an indication of a consistency of experimental technique combined with the ability of small delays to compensate for the differences. Thus the approximation to a sixth power function is not particularly important. Fig. 5*b* shows that an equation of the form of equation (3) will allow quite an adequate expression of the data of Fig. 5*a* by a variation of the delay time, t_0. It is also found that the same equation is applicable to the experimental conditions of Figs. 3 and 4 as shown by the agreement of the calculated circles with the data in Figs. 3*b* and 4*b*.

In view of its wide application, the extension of equation (5) has been investigated, mostly numerically, as a substitute for the HH counterpart, equation (2) and the expression for our earlier data, equation (4). In Fig. 7*a*, the equation

$$I = I_\infty\{1 - \exp[-(t + t_0)/\tau]\}^{25} \tag{6}$$

as shown by the curves, with appropriate values of t_0, has been compared with

$$I = I_\infty[1 - \exp(-t/\tau_x)]^x \tag{7}$$

for $x = 4$, 6, 10, 15 as given by the circles. The values of t_0/τ, n_0/n_∞, and τ/τ_g, given in Table I, were chosen to give the same values of t and dI/dt at $I = 0.5\ I_\infty$.

The maximum differences of a few per cent of I_∞ between equations (6) and (7) should be detectable but usually not obvious in experimental records. The qualitative difference between the time courses of the potassium current during the return to the resting potential after a depolarization seems likely to have been an important consideration in the choice of the original HH analytical formulation for this current. So for repolarization,

$$I = I_\infty\left[\frac{n_0}{n_\infty} + \left(1 - \frac{n_0}{n_\infty}\right)\exp\left(-t/\tau\right)\right]^{25} \tag{8}$$

has been compared with

$$I = I_\infty \exp\left(-xt/\tau\right) \tag{9}$$

for $x = 4$ and 6 where now $n = n_0$ and $I = I_\infty$ at $t = 0$, are the initial conditions for equation (8) at the start of the repolarization to n_0. The currents given by equation (9) initially decrease somewhat more rapidly and finally more slowly than those from equation (8) for τ/τ_g from Table I. But the two expressions agree throughout, as indicated in Fig. 7*b*, to within 5 per cent of the initial value and the depolarizations and repolarizations for $x = 4$ and 6 are to be compared with Fig. 2

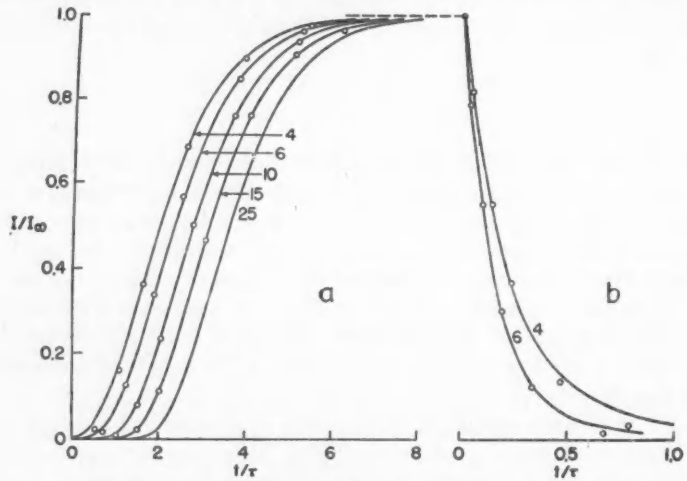

FIGURE 7a Potassium currents after depolarization computed by equation (6), solid lines where t_0 and τ have been adjusted to approximate equation (7). Circles are computed values of equation (7) for the exponents 4, 6, 10, and 15. FIGURE 7*b* Potassium currents after repolarization to initial conditions of Fig. 7*a* for exponents 4 and 6. The solid lines are computed by equation (8) and the circles by equation (9). Note change of scale for t/τ between Figs. 7*a* and 7*b*.

of HH IV. It seems unlikely that such experiments would produce decisive evidence against the use of equations (6) or (8).

The range of experimental conditions in the present work is somewhat limited but the ability of the new formulation to approximate the HH functions in their range of experimental success leaves little doubt that equation (6) will be equally valid in the ranges not here tested. It is true however that for general use, new values of n_∞ as a function of V will be required while from Table I the values of τ

TABLE I

x	4	6	10	15	25
t_0/τ	1.63	1.28	0.85	0.47	0
n_0/n_∞	0.804	0.722	0.572	0.375	0
τ/τ_x	0.928	0.955	0.977	0.988	1

will apparently need but little change. Some other modifications of the HH axon functions are anticipated in order to adapt them to the average of more recent data and this partial revision has not been undertaken.

The prospect of having to use a high power, such as 25 or above, for hand, analog, or digital computation makes such computations seem even more forbidding than with the original fourth power (HH IV; Cole, Antosiewicz, and Rabinowitz, 1955; FitzHugh and Antosiewicz, 1959). However, the approximate validity of the latter for depolarizations from the resting potential seems to justify this simplification as long as excessive hyperpolarizations are not encountered.

There is no reason to expect that the steady state conductance will ever become actually zero for any finite hyperpolarization so that this assumption should not be made for the —212 mv prepulse. Instead an exponent somewhat higher than 25 should be used with an appropriate delay at the highest hyperpolarization available and would probably be as satisfactory otherwise.

Since the number of other and equally satisfactory empirical equations is probably limited only by the ingenuity and patience and by the number of their inventors, this particular formulation cannot now be expected to have a unique significance, except perhaps that it is singularly pliable. Some years ago, for example, we found expressions of the form

$$\frac{1}{1 + (t/\tau_y)^{-y}}$$

and their hyperbolic tangent equivalents to be quite useful. With $y = 4$ these forms represent the early data of Fig. 2 a little better than does equation (4) and with $y = 5$ they are practically indistinguishable from Fig. 5*b* and equation (5). Thus a theory of ion permeability will probably be successful in explaining a vast amount of data to the extent that it approximates one of these equivalent forms.

Although the HH suggestion that n is the probability for one of four sites to be available is conceptually intriguing and the present modification to 25 may be more

indicative of a statistical distribution, there is no basis for such a comparison without a more detailed mechanism for either.

The ability of the equations

$$dn/dt = (n_\infty - n)/\tau; \qquad I = \bar{g}_K n^{25}(V - E_K)$$

to represent the data over almost the entire attainable ranges of V, n, m, h is very impressive. The extension of the dependence of n_∞ and τ upon V—and V alone—adds further weight to this already highly significant HH contribution. The unique I/I_∞ *versus* t/τ curve, where I_∞ and τ are completely determined by the membrane potential, becomes the more attractive as it is found that any and all initial conditions (except from a positive prepotential to one less positive) are shown as a displacement of this one curve along the time axis. As has been emphasized to us by Dr. FitzHugh, these results are highly indicative of a single variable of state and will follow if this variable is given by a first order differential equation. Less simple differential equations are not, however, excluded.

The time displacement approach may be of considerable theoretical significance but leads even now to some interesting qualitative speculations about physical mechanisms.

One may like to think that the membrane contains fewer and fewer potassium ions as it is increasingly hyperpolarized until it is nearly empty at perhaps a few hundred millivolts negative inside. Then on depolarization to 50 mv, positive inside, a front of ions advances across the membrane to appear as the beginning of a current after the time needed for the transit. If indeed the front was very sharp as it left the inner boundary of the membrane it would soon broaden by the diffusion superposed on the translation outward to give the gradual, delayed rise much as seen in Fig. 5*a*. For a lesser hyperpolarization the initial concentration would be higher at each point in the membrane and the gradient less steep. As a consequence the front would reach the outside sooner but might have much the same form because the lower initial gradient would also be spread less by diffusion in the shorter transit time. Intuitively satisfactory as this picture may seem, it cannot be confidently advanced to explain the observed near identity of current from extreme hyperpolarization to near E_{Na} until a supporting analysis is available.

It may, however, be assumed that the membrane is swept rather clear of ions at the highest hyperpolarization and that the time to half maximum current at the sodium potential approaches the transit time across the membrane. For a nominal membrane thickness of 100A, the average velocity is then $10^{-6}/0.6 \cdot 10^{-3}$ or $1.7 \cdot 10^{-3}$ cm/sec. The effective potential is $E_{Na} - E_K$ and the corresponding field is $0.12/10^{-6} = 1.2 \cdot 10^5$ v/cm. The mobility of $1.4 \cdot 10^{-8}$ cm/sec. per v/cm is thus about $2 \cdot 10^{-5}$ times the normal potassium ion mobility in water, $8 \cdot 10^{-4}$ in the same units. This is to be compared with an earlier estimate of 10^{-5} obtained by a somewhat different approach (Cole, 1947; 1949). However, the rate of rise observed is about a tenth that expected by diffusion on this basis.

Another possibility may be that the electric and concentration gradients combine in the membrane in such a way as to quickly form a characteristic concentration profile near the inner boundary. This might then be transmitted without change of form across the membrane, much as a boundary may move unchanged over long distances in a transference number determination. Appropriate analyses for such a steady state should be reasonably possible.

Apparent difficulties with these two suggestions arise from the fact that they are based on the Planck liquid junction model (1890). Even with the improvements of Goldman (1943), Teorell (1951), and Schlögl (1954) the steady state *V versus I* characteristic of the membrane should show a low ion rectification ratio equal to the ion concentration ratio across the membrane. Early measurements (Cole and Curtis, 1941) of the squid axon rectification were somewhat larger than the ion ratio and more recent ones (Cole and Moore, 1960) are considerably larger while there is no limiting value for the rectification ratio in the HH formulation. But the decisive evidence is from the squid axon in isoosmotic KCl. In this a negative resistance limb was found in the quasi steady state *V versus I* characteristic which does not appear in liquid junction theory but is as predicted by the HH empirical potassium conductance expression (Moore, 1959*a*). The possibility that such an effect may be produced by the electroosmosis factor, proposed by Teorell (1959), has not been investigated. But without some such modification, the liquid junction model should only be used with rather considerable reservations.

The constancy of current wave form also suggests a determining mechanism that is quite localized, perhaps at the inner face of the membrane, so that spatial variations along the ion path are relatively unimportant. In this case it may be somewhat more involved to have the mechanism controlled directly by the potential difference across the entire membrane. This difficulty is avoided in the pore distortion mechanism developed by Mullins (1959). Here the pores of a somewhat hyperpolarized membrane are closed enough by an electrostatic compression to block potassium ions. Upon depolarization the potassium permeability increases as the membrane relaxes to open the pores and allow these ions to pass. In his Fig. 11, Mullins gives a calculated potassium conductance curve that is quite similar to the experimental results. However, the delay is so much longer than the time of rise as to require an exponent of about 700 in place of the 25 appearing in equation (5). This difference can certainly be resolved by modification of already rather arbitrary assumptions.

Whatever may be the nature of the permeability controls, the apparent dependence of the potassium current characteristics upon potential alone—in spite of considerably varied sodium phenomena—gives additional support to the HH assumption that the potassium and sodium controls are quite independent of each other. It is of more than passing interest that evidence has not appeared to indicate a corresponding behavior of the sodium current in the range of considerable hyperpolarization.

In addition to the specific mention made of Professor Franck and Dr. FitzHugh, we wish to express our appreciation to them and to Drs. R. E. Taylor, W. J. Adelman, Jr., J. J. Chang, and Mr. J. H. Gebhart for their experimental, theoretical, and editorial assistance.

REFERENCES

COLE, K. S., 1947, Four Lectures on Biophysics, Institute of Biophysics, University of Brazil, 57.

COLE, K. S., 1949, *Proc. Nat. Acad. Sc.*, **35**, 558.

COLE, K. S., 1958, *Fed. Proc.*, **17**, 27.

COLE, K. S., ANTOSIEWICZ, H. A., and RABINOWITZ, P., 1955, *J. Soc. Ind. and Appl. Math.*, **3**, 153.

COLE, K. S., and CURTIS, H. J., 1941, *J. Gen. Physiol.*, **24**, 551.

COLE, K. S., and MOORE, J. W., 1960, *J. Gen. Physiol.*, **44**, 123.

FITZHUGH, R., and ANTOSIEWICZ, H. A., 1960, *J. Soc. Ind. and Appl. Math.*, **7**, 447.

GOLDMAN, D. E., 1943, *J. Gen. Physiol.*, **27**, 37.

HODGKIN, A. L., and HUXLEY, A. F., 1952*a*, *J. Physiol.*, **116**, 449.

HODGKIN, A. L., and HUXLEY, A. F., 1952*b*, *J. Physiol.*, **116**, 473.

HODGKIN, A. L., and HUXLEY, A. F., 1952*c*, *J. Physiol.*, **116**, 497.

HODGKIN, A. L., and HUXLEY, A. F., 1952*d*, *J. Physiol.*, **117**, 500.

MOORE, J. W., 1959*a*, *Nature*, **183**, 265.

MOORE, J. W., 1959*b*, *Proc. I.R.E.*, **47**, 1869.

MOORE, J. W., and COLE, K. S., 1961, *in* Physical Techniques in Biological Research, (W. L. Nastuk, editor), New York, Academic Press, Inc., **6**.

MULLINS, L. J., 1959, *J. Gen. Physiol.*, **42**, 1013.

PLANCK, M., 1890, *Ann. Physik u. Chem.*, **40**, 561.

SCHLÖGL, R., 1954, *Z. physik. Chem.*, **1**, N.S., 305.

TEORELL, T., 1951, *Z. Elektrochem.*, **55**, 460.

TEORELL, T., 1959, *J. Gen. Physiol.*, **42**, 847.

AN APPROACH TO THE QUANTITATIVE ANALYSIS OF ELECTROPHYSIOLOGICAL DATA FROM SINGLE NEURONS

GEORGE L. GERSTEIN *and* NELSON Y.-S. KIANG

From the Research Laboratory of Electronics, Massachusetts Institute of Technology, Cambridge, and the Eaton Peabody Laboratory of Auditory Physiology, Massachusetts Eye and Ear Infirmary, Boston

ABSTRACT The application of a digital computer to the processing of data from single neurons is described. Examples from experimental data are presented to demonstrate the usefulness of certain types of computations. These methods are placed in a descriptive mathematical framework. Other easily attainable computations are suggested.

INTRODUCTION

Since the days of Ramon y Cajal (1), the neuron has been generally accepted as the basic building block of the nervous system. This view has been important in the interpretation of electrical phenomena recorded in nervous tissue by macroelectrodes. Even the most careful of these recordings poses problems of measurement for which we lack satisfactory theoretical formulations. In the (more or less) intact animal, a macroelectrode records electrical activity from a volume that is large compared to that of a single neuron; the recorded activity is not of necessity functionally homogeneous. Thus there arises the problem of meaningfully relating the electrical activity seen by a macroelectrode to the underlying single neuron activity and, more generally, to a valid indicant of the behavior of the nervous system as a whole.

The introduction of microelectrodes has made it possible to obtain greater spatial resolution in recordings. It has become possible to record electrical events from a single nerve cell or even from certain regions of a given neuron. The temporal characteristics of these events cover the range of "fast" action spikes to DC and "slow"

This work was supported in part by the United States Army (Signal Corps), the United States Navy (Office of Naval Research), the United States Air Force (Office of Scientific Research, Air Research and Development Command), and Research Grant B-1344, National Institute of Neurological Diseases and Blindness, National Institutes of Health, Bethesda.

Dr. Gerstein is Postdoctoral Fellow of the Institute of Neurological Diseases and Blindness, National Institutes of Health, Bethesda.

Received for publication, August 3, 1960.

potential changes. Although any and all of these potentials may have functional significance (2-5), the action potentials or spikes have loomed largest, historically, in the analysis of single unit activity. Spatiotemporal patterns of spike activity have frequently been used as indices of nervous system function.[1] Such patterns have conveniently been studied in sensory systems because these systems are particularly accessible to manipulation.

In stimulus response studies, changes in spike activity must be assessed against a background of "spontaneous activity." Stimulation can lead to subtle changes of the temporal distribution of spikes. When these pattern changes occur with long latency and much variability, it hardly seems wise to define the "response" of a neuron as the casually detectable change in background activity that immediately follows stimulation. As closer and more formal examination of single-unit firing patterns becomes possible, the number of units that fall into the "no response" cate-

FIGURE 1 Spike and pulse trains discussed in the text. $R(t)$, single-unit activity (spikes) recorded by microelectrodes in cochlear nucleus; $f(t)$, idealization by pulse generator; $g(t)$, externally determined time marker.

gory diminishes strikingly. Potentially more useful categories can be obtained by more exact description of response pattern changes. For this purpose it appears necessary to utilize probabilistic approaches to the quantification of unitary spike activity.

It is the purpose of this paper (*a*) to illustrate, from our experimental work, the use of several methods of data processing which make possible the quantitative description of single neuron firing patterns and (*b*) to place these methods in a mathematical framework that makes explicit the interpretations that can be drawn from such analyses. We wish particularly to set forth both the power and the limitations of this approach to the description of firing patterns.

ANALYSIS OF SINGLE-UNIT DATA

If the time pattern of action spikes is selected as the subject of interest, other aspects of the electrical activity (such as details in the spike waveform, slow potentials) can be neglected. This selection is illustrated in Fig. 1 where $R(t)$ is a train

[1] Today it seems much less certain that the analysis of discrete events alone will lead to a complete understanding of the behavior of the nervous system. It is likely that an adequate description of nervous system activity can be obtained only through the analysis of *both* the graded electrical activity and the discrete spikes.

of spikes recorded by a microelectrode, and $f(t)$ is the idealization of $R(t)$ produced by letting the spikes trigger an electronic pulse generator. In such a train of identical pulses of unit amplitude all "information" is carried by the times at which individual pulses occur. In this article we shall consider the spike train $R(t)$ as being equivalent to the corresponding pulse train $f(t)$. In order to analyze the time structure of the train it is necessary to choose an origin (or a series of origins) for time measurements. There are two possibilities for this choice: (*a*) events in the spike train itself, or (*b*) externally determined instants (for example, $g(t)$ in Fig. 1).

The simplest application of the first choice leads to a class of analyses that we shall call "interval histograms;" the second choice leads to a class that we shall call "time histograms."

Within the past few years it has become possible to perform such computations on large masses of data with high resolution, accuracy, and speed. In order to obtain maximum flexibility in choosing the particular type of analysis to be used, it is convenient to work with a general-purpose digital computer. A data-processing system of this type which is in use at this laboratory has already been described (6). With this system, computations of the simplest cases of interval and time histograms have yielded useful analyses of single-unit firing patterns in several neurophysiological studies. In particular, we are using:

(a) an interval histogram—a histogram of the intervals between *successive* spikes.

(b) a poststimulus time (PST) histogram—the distribution of spikes in time relative to the instant of the *most previous* presentation of the stimulus, summed over many repeated stimulus presentations. A peak on an interval histogram shows a preferred interval between firings; a peak on a PST histogram shows a preferred time of firing relative to the stimulus.

(These analyses are, respectively, the second term of equation (3) and the first term of equation (7) below.)

It is not our intention to present the results of completed studies here; rather we wish to indicate certain advantages and disadvantages in the use of these and other methods for the analysis of single-unit data. All of our examples are drawn from work on the auditory system.

In order to formalize most simply the types of computation that we have used, let us assume that the basic spike train results from a process that is statistically stationary in the large. This means, if we are considering an experiment which involves the repeated presentation of the same stimulus, that we assume the statistical properties of all responses to be the same. In other words, we are examining a steady-state process and are not concerned with adaptation effects and other "dynamic" properties that could alter the response to successive identical stimuli. Within the time between presentations of the stimulus, the statistical properties of the process may of course vary. This assumption will avoid difficulties in choosing the segments of data over which calculations are made.

In this framework, interval histograms are selected portions of an estimate of the autocorrelation function for a train of suitably defined spikes. Let the spike train we are investigating be

$$f(t) = \sum_{k=1}^{N} \delta(t - t_k) \tag{1}$$

where $\delta(t)$ is a Dirac δ function (or, alternatively, a unit impulse), and where N is a large number. (For mathematical convenience we are representing the original train of *unit amplitude* spikes by a train of δ functions of unit area, each located at the time of an original spike. To interpret any results we must now consider *areas*.)

An estimate of the autocorrelation of (1) is

$$\varphi_{ff}(\tau) \equiv \int f(t)f(t - \tau)\, dt = \int \sum_{k=1}^{N} \delta(t - t_k) \sum_{l=1}^{N} \delta(t - t_l - \tau)\, dt$$

$$= \sum_{k=1}^{N} \sum_{l=1}^{N} \delta(t_k - t_l - \tau) \tag{2}$$

For convenience, the double sum can be broken up in the following way:

$$\varphi_{ff}(\tau) = N\,\delta(\tau) + \sum_{k=2}^{N} \delta(t_k - t_{k-1} - \tau) + \sum_{k=3}^{N} \delta(t_k - t_{k-2} - \tau) + \cdots . \tag{3}$$

These terms correspond respectively to letting $l=k$, $l=k-1$, $l=k-2$, . . . Since the autocorrelation function is symmetric in τ, we have not written the $-\tau$ terms explicitly.

Thus the estimate of the autocorrelation function of (1) is itself expressed as an array of δ functions. The numerical values of the estimated autocorrelation function would be obtained from the envelope of the δ function *areas*.[2]

For convenience we may measure the continuous values of τ as discrete time values τ_j, $j=1, 2, 3, \ldots$, in such a manner that all τ that satisfy $\tau_j<\tau<\tau_{j+1}$ are measured as τ_j. Thus $\tau_{j+1}-\tau_j \equiv \Delta\tau$ defines a time bin that determines the resolution of the analysis. The choice of bin width is governed by the time scale of the particular phenomena that are being studied. In this case of discrete time values, the *areas* of all δ functions of φ_{ff} which fall between τ_j and τ_{j+1} are added together to give the height of the τ_j—th bar in a histogram.

The first term of equation (3) is a constant contribution to the estimated autocorrelation function at $\tau=0$; its numerical value (area) is N, the total number of spikes in the train. If the time duration of the spike train is known, this term of equation (3) yields the average firing rate in the spike train. The second term is an interval histogram; *i.e.*, a histogram of the intervals between *successive* (k and $k-1$) spikes of the train. The

[2] This usage is common in text-books. See chapter 2, reference 7. The reader who finds our notation obnoxious can perform a similar development in terms of summations only, without using δ functions, integrals, or integral properties, by starting with a spike train

$$f(t_i) = \sum_{k=1}^{N} \Delta(t_i - t_k) \quad \text{where} \quad \Delta(t_i - t_k) = \begin{matrix} 1,\ t_i = t_k \\ 0,\ t_i \neq t_k \end{matrix}.$$ For discrete time shifts τ_m, equation (2) would be $$\varphi_{ff}(\tau_m) = \sum_{k=1}^{N} \sum_{l=1}^{N} \Delta(t_k - t - \tau_m).$$ Interpretation of results in terms of areas is then unnecessary. Still other forms of notation are possible. However, the particular resolution of components expressed in (3) and (7) remains valid.

third term is an interval histogram of the intervals between every second (k and $k-2$) spike. All subsequent terms are interval histograms for higher order intervals in the spike train.

A peak on an interval histogram shows a preferred periodicity in the train; *i.e.*, a preferred interval between spikes or groups of spikes. The value of this preferred interval is indicated by the position of the peak on the abscissa. The ordinate measures the number of spike intervals falling into each discrete τ_j time bin.

In a similar manner, the time histograms are selected portions of an estimated cross-correlation function between the spike train under study and an external pulse train that can be determined arbitrarily by the experimenter. Again, let the spike train that we are investigating be

$$f(t) = \sum_{k=1}^{N} \delta(t - t_k) \tag{4}$$

and let the externally determined (not necessarily periodic) pulse train be

$$g(t) = \sum_{l=1}^{N} \delta(t - t_l) \tag{5}$$

Generally, very few, if any, t_k and t_l will have the same values. An estimate of the cross-correlation function of functions (4) and (5) is

$$\varphi_{fg}(\tau) \equiv \int f(t)g(t - \tau)\, dt = \int \sum_{k=1}^{N} \delta(t - t_k) \sum_{l=1}^{N} \delta(t - t_l - \tau)\, dt$$

$$= \sum_{k=1}^{N} \sum_{l=1}^{N} \delta(t_k - t_l - \tau) \tag{6}$$

Although (6) looks formally like (2), the t_k and t_l are *not* the same series in this case, and the double sum cannot be broken down as in (3). Instead we write

$$\varphi_{fg}(\tau) = \sum_{l=1}^{N} \left[\sum_{\substack{k \\ t_l < t_k < t_{l+1}}} \delta(t_k - t_l - \tau) + \sum_{\substack{k \\ t_k > t_{l+1} \\ t_k < t_l}} \delta(t_k - t_l - \tau) \right] \tag{7}$$

Thus the estimate of the cross-correlation function is also expressed as an array of δ functions. Just as for equation (3), the numerical values are obtained from the envelope of δ function *areas*.

As in the discussion of equation (3), the continuous τ can be measured as discrete τ_j, $j=1, 2, \ldots$

The two right hand terms of equation (7) are time histograms; *i.e.*, histograms of the average times of occurrence of the $f(t)$ spikes relative to origins determined by the external $g(t)$ pulses. The first term describes the average times of occurrence of the $f(t)$ spikes relative *only* to the last previous (lth) $g(t)$ pulse as origin. The second term lumps together the average times of occurrence of the $f(t)$ spikes relative to the $l-1$, $l-2$, $\ldots$, $g(t)$ pulses. In other words, a peak on a time histogram shows, on the average, a preferred time of occurrence of the $f(t)$ spikes relative to the $g(t)$ pulses. The value of this preferred time is indicated by the position of the peak on the abscissa. The ordinate measures the number of spikes that fall into each discrete time bin.

This computation serves to sort the spike train under study in a way that detects pat-

terns that are time-locked to the arbitrary external pulse train. Suppose, for example, that the arbitrary external pulse train marks the delivery of stimuli. Then the first term of equation (7) would detect average evoked response patterns that occur during the time *before* the delivery of the next stimulus. Let us call this particular computation a poststimulus time (PST) histogram. If the perturbations caused by the first stimulus have not died away by the time the next stimulus is delivered, a part of the pattern that is time-locked to the stimulus would be found in the second term of equation (7). (The physical meaning of the two terms of (7) is most easily visualized in the case in which the stimuli are delivered aperiodically but at a mean interval that is shorter than the duration of the time-locked evoked response pattern.)

We cannot overemphasize that both types of histogram that have been discussed involve averaging the data. This means that in performing these computations, to bring out certain aspects of the spike pattern, we have lost other information. For example, we lose the time sequence of the events contributing to a particular histogram. This could be remedied, in principle, by computing separate time and interval histograms for the first, second, ... , spike, or spike pair after the stimulus. Unfortunately, there are so few data in most experiments that such fractional analyses are statistically impractical.

A far more crucial loss of information is hidden in the assumptions involved in averaging: a meaningful average can be obtained only if the events in the pattern that enter into the average have statistical properties which are similar. If the statistical properties of the events vary during the period of the average, then an "average" of the events can still be computed, but there will be a loss of all information about the changes of the statistical properties. In any real neurophysiological experiment such changes of the statistical properties are associated with inevitable physiological variability. Thus a more complete description of the properties of neural firing patterns must eventually necessitate the use of higher order statistical measures.

There is an interesting difference in the interpretation of the two general types of histogram. In the time histogram, we seek significant variations of the distribution as a function of poststimulus time—a distribution that is flat within statistics, *i.e.*, a DC contribution conveys little of interest. Such a flat distribution represents the events in the spike pattern which are not time-locked to the external pulse train, and which are therefore randomly distributed in time relative to the external train. For the interval histogram, however, all parts of the distribution are pertinent because no criteria external to the spike train are used in the computation.

EXPERIMENTAL METHODS

All experiments were performed on cats anesthetized with either dial or nembutal, given either intraperitoneally or intravenously. Recordings were made from one of two places: (*a*) the cochlear nucleus, or (*b*) the auditory cortex. The cochlear nucleus was approached through the intracranial route with removal of cerebellum. Cortical recordings were made with a closed chamber technique similar to that described by Davies (8). Electrodes were either the indium-platinum type described by Dowben and Rose (9) or the tungsten type described by Hubel (10). In all cases the experiments were conducted in sound-proof chambers, with hydraulic remote control of the microelectrode. Clicks were delivered by a PDR-10 earphone connected to the external auditory meatus through a plastic tube. The intensity of the clicks is stated relative to the VDL (visual detection level), of the appropriate evoked response as recorded by a macroelectrode.

Responses were recorded with an FM tape system. For the cortex both a high-pass (200 to 10 kc) and an "unfiltered" (8 to 10 kc) channel were recorded. This allowed investigation of both unit spike potentials and slow potentials.

The processing of single-unit data by the TX-O general-purpose digital computer has already been described. (6) Output from the computer was obtained as a display of a bar graph and titles, and was photographed with a Polaroid camera.

RESULTS AND DISCUSSION

The fundamental objective of our experimental work is the detection of changes that take place in single neuron activity patterns as a result of changes in stimulus conditions. Neurophysiological spike trains can be considered in two categories: *(a)* spontaneous activity, and *(b)* responses to stimuli. Any stimulus condition results in a spike pattern that is a mixture or interaction of both types of activity. The effect of a discrete stimulus on the over-all spike pattern decreases with time after stimulation; the pattern gradually returns to the spontaneous condition. If the stimuli are spaced far apart in time, the over-all contribution of the stimulus-dependent activity (responses) is low relative to the spontaneous activity. If stimuli are delivered at sufficiently high rates, the contribution of spontaneous activity can become relatively small.

The interval histogram emphasizes *internal* timing relations in the spike train, whether the individual spike be spontaneous or in response to a stimulus. The PST histogram emphasizes the time relations of the spikes in the train to the stimulus time marker.

In general, the spike trains with which we deal represent some interaction of spontaneous and responsive activity, so that both the interval and time histograms are useful in describing the patterns of activity.

In practice, for particular samples of data, we have found that one or the other display is more striking in showing differences in activity patterns. This contrast in effectiveness between the two displays can be attributed to the relative contribution of spontaneous and responsive activities.

Figs. 2 and 3 show applications of interval histogram computations. Fig. 2*a* shows single-unit activity recorded from the cochlear nucleus during various rates of click presentation. Note that the unit exhibits spontaneous activity that appears to be suppressed when clicks are delivered at rates around 10 or 20/sec. At 10/sec. the unit appears to fire once and only once to each click. At 20/sec. there appear to be some clicks to which the unit does not respond, although whenever a spike occurs it seems time-locked to the stimulus. Over considerable stretches of time the unit appears to fire to every other click.

At higher rates, from these pictures, it becomes more difficult to describe the pattern of activity with respect to the stimulus. On a faster time base, there appears to be some following with irregular skipping.

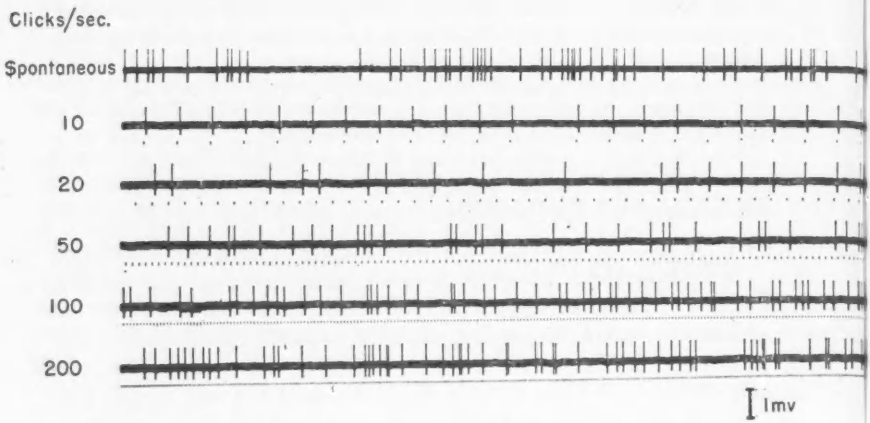

FIGURE 2*a* Activity of a single unit in cochlear nucleus (unit 165-1) during presentation of clicks at various rates. Click intensity 25 db re VDL.

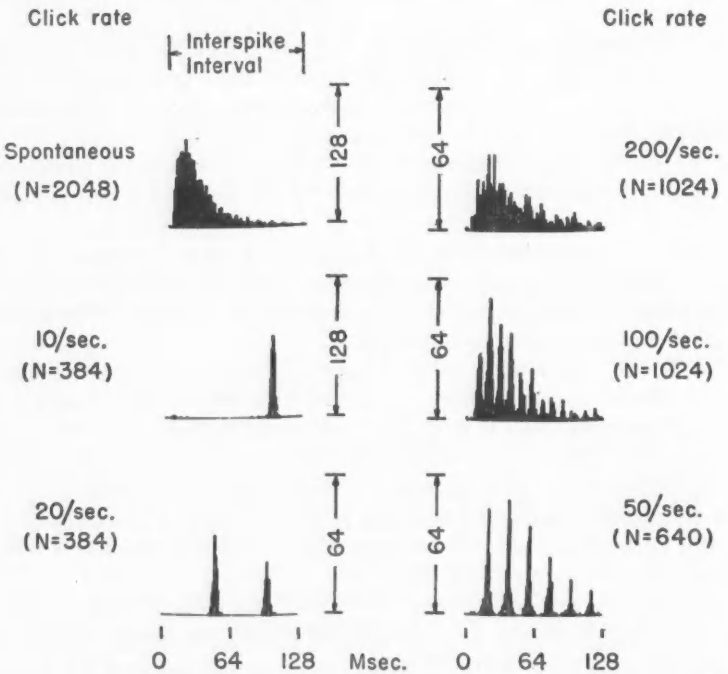

FIGURE 2*b* Interval histograms of the same data from which Fig. 2*a* was obtained. The ordinate on all displays is the number of spikes per unit time interval. *N* is the total number of spikes represented in each histogram.

Fig. 2*b* shows the interval histograms for the same samples of data from which Fig. 2*a* was taken.

The interval histograms show very clearly the marked effect of 10/sec. clicks on the pattern of spontaneous activity. The single sharp distribution at 100 msec. (*i.e.*, time interval between clicks) reflects the one-to-one following seen in Fig. 2*a*. For 20/sec., there is one large peak at 50 msec. (*i.e.*, time interval between clicks) and an additional smaller peak at 100 msec. which corresponds to those intervals when the response skips one stimulus. The relative areas of the two peaks expresses the relative number of times that the unit responds in a one-for-one manner as compared with the number of times that the unit skips one stimulus. Note especially that there is negligible activity with intervals other than at the periods of the stimulus or its subharmonics. At 50/sec. the fundamental period of the stimulus is 20 msec. The first peak in the interval histogram corresponds to this period (*i.e.*, one-for-one responses). Now however, the second peak, representing intervals of 40 msec., is larger than the first peak. This signifies that the unit now fires more often to every other click than to every click. The areas of the peaks at higher interval values indicate the relative occurrence of activity which skips two, three, etc., clicks. At 100/sec., similar observations can be made. At 200/sec., while the individual peaks are no longer clearly separable, the envelope of the interval distribution approaches that of spontaneous activity. It is evident that the interval histogram emphasizes certain "interesting" features of the pattern not easily studied in the original records.

Fig. 3 shows interval histograms for a unit in the auditory cortex (A1). The

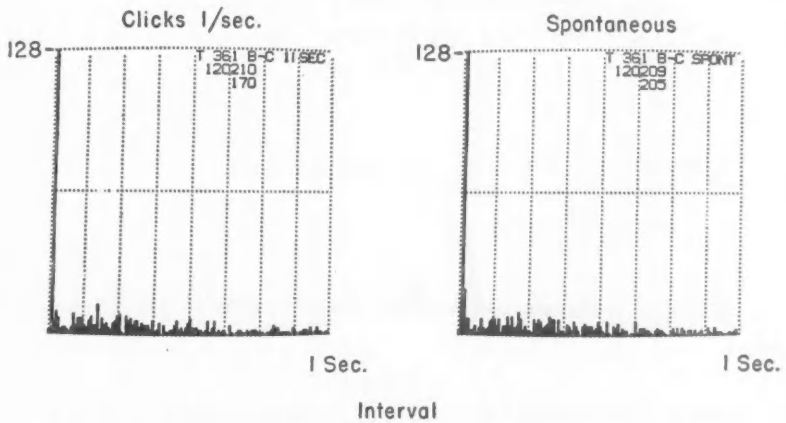

FIGURE 3 Interval histograms for a unit (120-2) in auditory cortex. Left, activity during click presentations. Right, activity during the interleaved spontaneous conditions. Click intensity 20 db re VDL. $N = 576$.

large peak at small interval corresponds to the rapid bursts of 2 or 3 action potentials which were characteristic for this unit. These displays do not show any gross differences between the stimulated and unstimulated conditions. However, observation of the unit's activity during the experiment seemed to indicate that the stimulus had some effect, although there was much spontaneous activity. The similarity of the interval histograms for 1/sec. clicks and the spontaneous condition is probably a reflection of the relatively large "spontaneous" contribution to the over-all activity even during stimulation. This picture is true for most cortical units that we have observed even at higher click presentation rates. The interval histogram does not clearly reflect changes in the pattern of most of our cortical unit responses. Comparison of Figs. 2 and 3 shows that, determined by the particuliar behavior of a unit, the interval histogram may or may not be trivial.

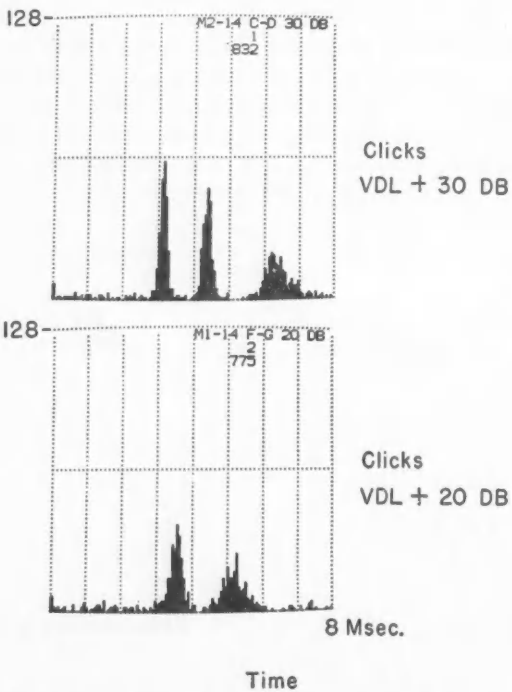

FIGURE 4 PST histograms for a unit in cochlear nucleus (unit K — 173 — 3). Top, activity during presentation of clicks at 30 db re VDL. Bottom, activity during presentation of clicks at 20 db re VDL. $S = 256$, the number of stimulus intervals processed.

Various applications of the time histogram display are shown in Figs. 4 to 6. In each case the time of stimulus presentation or dummy time marker is at the extreme left of the histogram.

Fig. 4 shows the time histogram for a cochlear nucleus unit when two intensities of clicks are used. Under these conditions photographs of the responses show that

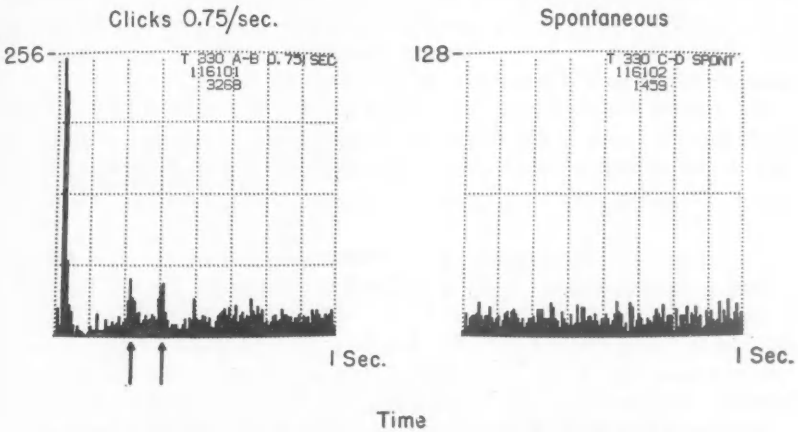

FIGURE 5 PST histograms for a unit in auditory cortex (unit 116-1). Left, activity during clicks presented at 0.75/sec. Right, spontaneous activity. Click intensity 20 db re VDL. $S = 512$.

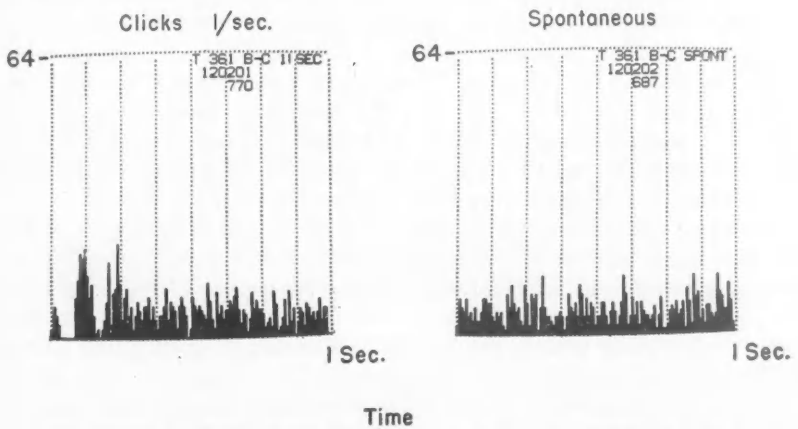

FIGURE 6 PST histograms for the same data as Fig. 3 (unit 120-2 in auditory cortex). Left, activity during clicks presented at 1/sec. Right, interleaved spontaneous activity. $S = 256$.

206829

the unit fires repetitively to each click. The number of repetitives may not be constant. The area under a particular peak in the PST histogram relates to the number of responses that may be identified as that particular repetitive. The increasing width of successive peaks indicates the increasing time jitter of successive repetitives. Not only does the PST histogram show an increase in the number of repetitives with increased stimulus intensity but it also shows that *(a)* the latency of the first response decreases; *(b)* the time between the first response and the first repetitive response decreases; and *(c)* the time distributions become sharper. These features are very difficult to detect in an interval histogram display.

Fig. 5 shows PST histograms for a cortical unit that responds to 0.75/sec. clicks. Here, there is a peak in the distribution around 20 msec. and some evidence for time-locking of later activity in the two peaks indicated by arrows. Immediately after the large first peak there appears to be a relatively silent period of about 150 msec.

Fig. 6 shows PST histograms for a unit whose most apparent reaction to clicks is a silent period followed by a peak in the distribution around 110 msec. This strikingly display of the effect of the stimulus should be contrasted with the corresponding interval histograms of Fig. 3. The samples of data processed for Figs. 3 and 6 are the same. Thus the PST histograms always selects activity time-locked to the stimulus, although it is of little value in studying ongoing spontaneous activity.

We have found the interval and PST histograms useful even in the analysis of response patterns from unanesthetized animals, in which the spontaneous activity is extremely labile.

The type of single-unit data processing that we have used can be advantageously combined with other computational methods in certain problems. For example, Fig. 7 is from a study of the relationship between slow waves and action potentials observed by the same microelectrode. The spikes, for various rates of click presentation, were analyzed by PST histograms. The slow wave activity during the same time was averaged by the ARC computer (11) and is, in each case, plotted above the histogram. The parallel course, in this particular case, of the average PST neuron firing rate and the average of the slow wave is thus made apparent.

There are other computational methods that can be applied to the study of unit activity. As has been shown in the mathematical section, a more complete description of spike trains can be achieved by computing the remaining terms of equations (3) and (7). When these terms in equation (3) (interval histogram) are computed, it is possible to study the distribution of *groups* of spikes. In the case of PST histograms, the additional terms in equation (7) will show the effects of one stimulus that last beyond the instant of presentation of the next and subsequent stimuli. This makes possible the study of responses to patterns of stimuli.

Another extension of our analytical tools is to set more complex criteria for the time markers in the averaging procedures for computing time histograms. This will

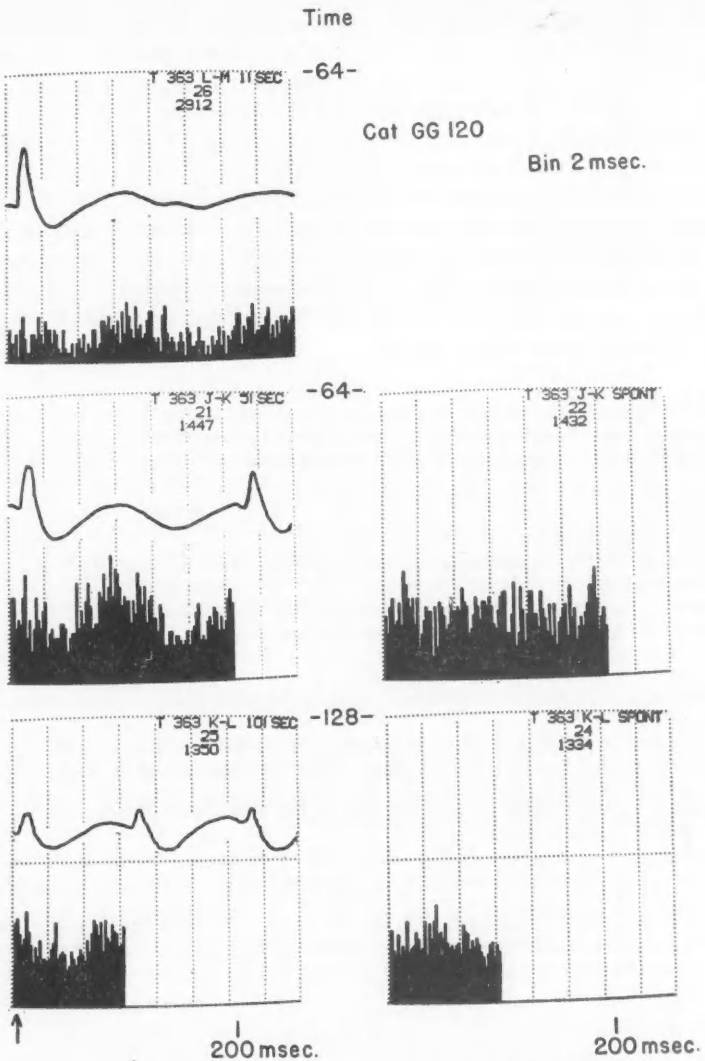

FIGURE 7 PST histograms for a unit in auditory cortex (unit 120-1). Left, activity during presentations of 1, 5, 10 clicks/sec., top to bottom. Right, interleaved spontaneous activity. The curves are the average of the slow activity measured by the same microelectrode during the same time. Click intensity 20 db re VDL. $S = 512$; 1536; 2560 respectively, top to bottom.

enable study of response probabilities which are conditional on certain aspects of the response. In Fig. 4 for instance, one could study the dependence of the latency of the first response on the occurrence of repetitives to the preceding stimulus.

As experimental methods begin to permit the simultaneous recording of many functionally connected neurons, it will become necessary to investigate various conditional statistics between the several activity patterns.

These particular extensions over our present work are relatively easy to achieve with the general-purpose computers that we are using. Complete descriptions of the time properties of a spike train involve variances and other higher order statistics that cannot be discussed here. But the various computation techniques we have outlined begin to permit quantitative tests of specific mathematical models of the properties and interactions of single neurons.

We should like to thank Professor W. A. Rosenblith for his continued advice and interest in these problems, and R. M. Brown for help with problems of instrumentation. We are grateful for the technical assistance of the staffs of the Research Laboratory of Electronics, Massachusetts Institute of Technology, and the Eaton Peabody Laboratory, Massachusetts Eye and Ear Infirmary.

REFERENCES

1. RAMON Y CAJAL, Recollections of My Life, Philadelphia, American Philosophical Society, 1937.
2. GRANIT, R., Receptors and Sensory Perception, New Haven, Yale University Press, 1955.
3. BULLOCK, T. H., Neuron doctrine and electrophysiology, *Science*, 1959, **129**, 997.
4. ROSENBLITH, W. A., Some quantifiable aspects of the electrical activity of the nervous system, *Rev. Mod. Physics*, 1959, **31**, 532.
5. ADRIAN, E. D., The Basis of Sensation. The Action of Sense Organs, London, Christophers, 1928.
6. GERSTEIN, G. L., Analysis of firing patterns in single neurons, *Science*, 1960, **131**, 1811.
7. MASON, S., and ZIMMERMANN, H., Electronic Circuits, Signals, and Systems, New York, John Wiley & Sons, 1960.
8. DAVIES, P. W., Chamber for microelectrode studies in the cerebral cortex, *Science*, 1956, **124**, 179.
9. DOWBEN, R. M., and ROSE, S. E., A metal filled microelectrode, *Science*, 1953, **118**, 23.
10. HUBEL, D., Tungsten microelectrode for recording from single units, *Science*, 1957, **125**, 549.
11. Communications Biophysics Group of the Research Laboratory of Electronics, and W. M. Siebert, Processing Neuroclectric Data, Technology Press Research Monograph and Technical Report 351, Cambridge, Research Laboratory of Electronics, Massachusetts Institute of Technology, 1959.

THE ULTRAVIOLET LIGHT INACTIVATION OF ΦX174 BACTERIOPHAGE AT DIFFERENT WAVE LENGTHS AND PH'S

RICHARD SETLOW *and* RICHARD BOYCE

From the Biophysics Department, Yale University, New Haven

ABSTRACT The bacterial virus, ΦX174, which contains a single strand of DNA has been inactivated by different wave lengths of monochromatic ultraviolet light at pH 7, 2, and 12. The action spectra for inactivation at these three pH's all showed minima at 2400 A rather than at 2300 A, which is the characteristic absorption minimum of DNA. The shapes of the action spectra have been analyzed in terms of the effects of absorbed light on the pyrimidines and purines rather than the effect on nucleoprotein. In this interpretation the pyrimidines are *at least* 2 to 3 times more sensitive than the purines. The quantum yield for inactivation of the virus at 2650 A and pH 7 is 0.006. The quantum efficiency for quanta absorbed in the pyrimidines is 0.0085 and for the purines 0.0035. It is pointed out that action spectra for single- and double-stranded polynucleotides should have minima at different wave lengths, and that this difference may be used to distinguish between these two configurations *in vivo*.

The small bacterial virus ΦX174 contains a DNA polynucleotide which is single-stranded (1). It will be useful to know the relations and differences between the physical properties of single- and double-stranded DNA. Such differences are not only of interest in their own right, but also may provide physical means for distinguishing between single- and double-stranded DNA *in vivo*. The effects of radiation on a single-stranded DNA may be simpler to analyze than those on the double-stranded configuration because of the smaller likelihood of energy migration up and down the single-stranded chain. It should be possible, by analyzing the effects of different wave lengths of ultraviolet (UV) light on ΦX174 irradiated at different pH's, to assess the relative importance, in the inactivation process, of quanta which are absorbed in the various bases of DNA. The data to be presented on the inactivation of ΦX174 may explain the action spectra obtained for more complex biological systems.

This work was assisted in part by a grant from the United States Public Health Service No. 1285-C3.

Received for publication, April 28, 1960.

Studies of the effects of UV light on biologically inactive polynucleotides have indicated that the pyrimidines are altered more rapidly than the purines (2, 3). One might expect, therefore, that for single-stranded DNA the action spectrum for the destruction of biological activity would follow the absorption spectrum of the pyrimidines rather than the absorption spectrum of the purines plus pyrimidines. This seems to be the case for ΦX174. By changing the pH of the medium it is possible to make large changes in the absorption spectra of thymidine and cytosine deoxyriboside. From the changes in the action and absorption spectra with pH it is possible to assess the relative importance of these two bases in the inactivation process. The resolution of the action spectrum for ΦX174 into the sum of component bases is similar in principle to the resolution of the action spectrum for the inactivation of enzymes into the sum of two parts, one representing an effect on the amino acid cystine and the other on the aromatic groupings in the molecules (4).

The differences between the action spectra for single-stranded DNA and double-stranded DNA may make it possible to distinguish between biological processes which take place *via* the single- *versus* the double-stranded configuration (5). Such differences in action spectra have been observed in the inactivation of complexes of bacteriophage T2 and *Escherichia coli* at various times in the latent period and have been interpreted in terms of a change in the configuration of viral DNA from the double- to single-stranded configuration (6).

EXPERIMENTAL PROCEDURE

The virus ΦX174 and the sensitive host cells (*E. coli strain* C) were obtained from I. Tessman. In the work reported here, the virus used for irradiation was obtained from a single lysate inoculated with virus from a single plaque. The general techniques of assaying and handling the virus are described by Zahler (7). Dilutions, after irradiation, were made into Difco nutrient broth. Plates were incubated at 37°C in the dark.

The virus for irradiation was diluted over 500 times from the lysate medium (tryptone, glucose, yeast extract) into the appropriate buffer, and, as a result, the absorption of the irradiated samples was less than 20 per cent. The initial virus titer for irradiations was between 10^7 and 10^8 plaque-forming units per ml. Three irradiation media were used: pH 7, obtained with 0.07 M phosphate buffer; pH 2, obtained with HCl-KCL buffer; and pH 12, obtained with 0.01 M NaOH. Control samples of the virus were not inactivated in these media for times equal to the duration of an experiment.

Monochromatic light was obtained from a large water prism monochromator (8). The intensity at each wave length was measured with a photocell which had been calibrated in absolute units. The average intensity throughout the sample, which was irradiated in a 1.0 cm light-path quartz cell kept at 15°C, was obtained from the incident intensity by using the corrections calculated by Morowitz (9). During irradiation the virus suspension was stirred with a small magnetic stirrer. Intensities ranged from 3 ergs/(mm² sec.) at 2650 A to 0.1 erg/(mm² sec.) at 2262 A. Irradiation times ranged from a total of 5 minutes at the high intensities to 40 minutes at the low intensities.

The inactivation of the virus depended only on the product of the intensity and the

time for intensities, at 2650 A, which varied over a factor of 20. There was no observed recovery of the virus on standing 18 hours at 4°C at pH 2. (Such a recovery might be expected from the fact that the UV photolysis of cytosine shows a rapid reversible effect at low pH's (10).)

RESULTS AND DISCUSSION

Action Spectrum at pH 7. Typical data for the inactivation of ΦX174 at pH7 are shown in Fig. 1. It is seen that the relative survival, over a factor of 10^4, decreases exponentially with the incident dose of radiation. There is no evidence for a slight shoulder at low doses, as is found for T2 bacteriophage, or for a decrease in sensitivity at high doses as found for T1 bacteriophage (11). This fact

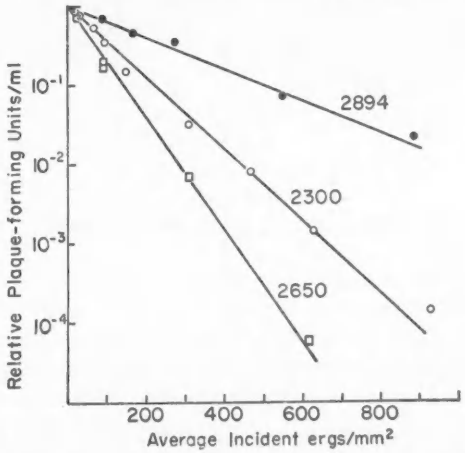

FIGURE 1 Dose-survival curves for ΦX174 at pH 7 for several different UV wave lengths.

makes it a relatively simple matter to obtain precise values for the sensitivity of the virus to UV inactivation. The data shown in Fig. 1 may be represented by the expression

$$n/n_0 = e^{-\sigma D}$$

where n/n_0 represents the relative survival of the virus, D the incident radiation in quanta/cm², and σ the sensitivity parameter which, because it has the dimensions of cm²/quantum, will be called the inactivation cross-section. The inactivation cross-section may be found from the slopes of the curves shown in Fig. 1 after the data have been converted to quanta/cm². The values of σ obtained in this way are precise. For example, four inactivation runs at 2650 A similar to that shown in Fig. 1

gave a mean value of σ for which the probable error of the mean was 0.7 per cent. The fewer repeat runs which were carried out at other wave lengths indicated probable errors of less than 5 per cent. In this experiment, because of the difficulties of determining absolute intensities over a wide wave length range, the biological error appears to be less than that associated with the physical measurements.

A graph of the inactivation cross-section *versus* wave length is the action spectrum. Fig. 2*a* shows the action spectrum for the inactivation of ΦX174 irradiated at

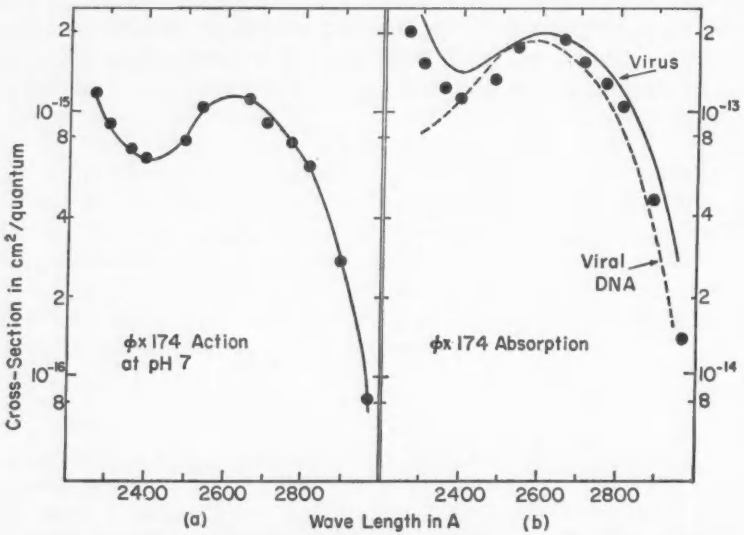

FIGURE 2*a* The action spectrum for inactivation of ΦX174 at pH 7. FIGURE 2*b* The absorption spectrum of the virus and of viral DNA from reference (1). The *relative* action spectrum, shown by the solid points, has been shifted so as to coincide with the absorption spectrum at 2650 A.

pH 7. Each point in this spectrum is obtained from an inactivation curve similar to the curves shown in Fig. 1. Fig. 2*b* shows, for comparison, the absorption spectrum of the virus, and of the viral DNA recalculated from data obtained by Sinsheimer (1). The absorption coefficient has been expressed in terms of the absorption cross-section per molecule, *s*, which is defined from the equation

$$I/I_0 = e^{-nsx}$$

where I/I_0 is the relative light transmission through a sample of thickness x with n units/cm³. In Fig. 2*b*, the action spectrum has been shifted so as to coincide with the virus absorption spectrum at 2650 A. The efficiency of *absorbed* photons in inactivating the virus may be expressed in terms of the quantum yield—the number

of virus particles inactivated per quantum absorbed. It may be found from the ratio of the inactivation cross-section σ, to the absorption cross-section (4):

$$\phi = \sigma/s. \tag{1}$$

On the logarithmic scale shown in Fig. 2 the action and absorption spectra are *not* parallel. Therefore the quantum yield at pH 7 is *not* independent of wave length but varies as shown in Fig. 3. At 2650 A its value is 0.006, which means that one out of 170 absorbed quanta inactivates the virus. This is a high efficiency compared to the efficiencies obtained for larger viruses T2 and T1 bacteriophages which have quantum yields of 3×10^{-4} and 6×10^{-4} respectively (12).

Of more interest than the absolute values of quantum yields is the fact that the action spectrum does not have the same shape as the absorption spectrum of either

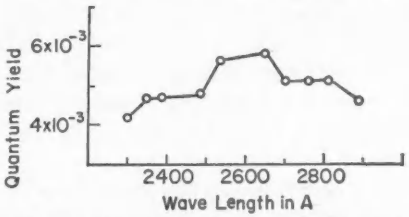

FIGURE 3 The quantum yield as a function of wave length at pH 7.

the virus or the viral DNA. The quantum yield is not constant if computed, as in Fig. 3, on basis of quanta absorbed in the virus or, as may be seen from Fig. 2, if computed on the basis of quanta absorbed in the nucleic acid portion of the virus. There are two possible extreme interpretations of the variation in ϕ with wave length. One is that both the protein and nucleic acid parts of the virus are sensitive to ultraviolet light and by choosing the sensitivity of these components appropriately we can obtain the observed action spectrum. Against this interpretation are the facts that all enzymatic proteins need much larger incident doses of radiation to affect them (13) than are used to inactivate the virus, and that there is no evidence for energy transfer from proteins to nucleic acids (14). Moreover, while the increase in virus sensitivity at wave lengths below 2400 A may be explained in terms of light absorbed in protein, the decrease at 2480 and 2400 A is inexplicable in these terms. If, therefore, we reject the possibility that the action spectrum for inactivation of ΦX174 is nucleoprotein in nature, we are left with the second possibility—a description of the action spectrum in terms of the sum of effects on the different bases which make up the DNA of ΦX174.

Analysis in Terms of the Effects on Individual Bases. It is reasonable to assume, from the results of the irradiation of free bases and polynucleotides (ably reviewed in reference 3), that the pyrimidines are the most sensitive units. Therefore, we shall attempt to describe the action spectrum in terms of a sum of light-

action on the cytosine and thymine components. There exist conceptual difficulties to this analysis. First, it is known that the effects of light on the free bases are wave length–dependent. Effects produced by longer wave lengths are at least partially reversible and those produced by wave lengths below 2300 A are irreversible (15). The relative magnitudes of these two wave length sensitivities are not known and we do not know how to evaluate the different rates of the reverse reactions in irradiated cytosine and thymine (16). Second, if we wish to analyze the spectrum in terms of the individual bases, we must assume, in the absence of more detailed information, that the bases act as independent absorbers. This is only approximately true for ΦX174-DNA because the absorption spectrum of the extracted DNA changes with the configuration of the molecule (1). The increase in extinction upon hydrolysis is, however, only 11 per cent compared to the increase of 30 to 35 per cent observed for double-stranded DNA.

We list below the explicit assumptions we shall make in order to arrive at a simple description of the effects of ultraviolet light on ΦX174. As we indicated above, these assumptions are known to be only approximately true where data relating to them are available. Therefore, it should not be suprising if the analysis yields only approximate results.

1. The bases are independent of one another and of the protein shell.

2. The quantum yield for affecting an individual base is independent of wave length.

3. The quantum yield for affecting a base at a particular wave length is independent of pH. (See reference 3 for evidence against this assumption.)

4. The ionization of the bases inside the virus is the same as if they were in the external solution.

As the pH is decreased from 12 to 2, the pyrimidine but *not* the purine nucleotides show big changes in absorption spectra (17). In going from pH 7 to 2 the absorption spectrum of cytosine changes, whereas that of thymidine does not. And the absorption spectrum of thymidine changes if the pH is raised from 7 to 12, wheras cytosine shows only a minor change. At this high pH guanosine's absorption spectrum changes slightly, but we shall ignore this change. (We note in passing that the changes in the guanosine absorption, an increase at 2700 A and a decrease between 2600 and 2300 A, do *not* agree with the changes in the action spectrum.) Fig. 4 shows the spectra of the two pyrimidines at the pH's we are interested in. The molar ratio of thymidine to cytosine in ΦX174 is 1.6 to 1 (1). Fig. 5 shows the computed absorption spectrum of a mixture of thymidine and cytosine in these ratios at the three pH's of interest. We would expect, if our limiting assumptions held, and if the pyrimidines are the most sensitive bases, that the action spectra of the virus at these three pH's would look like the absorption spectra shown in Fig. 5. At the beginning of the analysis it is worth noting that at pH 7, as a comparison of Figs. 2 and 5 shows, the action spectrum for inactivation of the virus does *not* look like the sum of thymine plus cytosine absorption. It shows a disproportionately

higher sensitivity at wave lengths below 2400 A which may be due to the increase in quantum yield of the individual bases at these wave lengths.

Action Spectra at pH 2 and pH 12. Fig. 6 shows the action spectra, determined from data similar to those shown in Fig. 1, for the inactivation of ΦX174 at pH 2, 7, and 12. The changes in the action spectra from the values at pH 7 are not drastic but, because of the high precision of the data, the differences in the spectra are significant. Thus, for example, at pH 2, cytosine's absorption coefficient at 2400 A decreases drastically and we find that the UV sensitivity has also de-

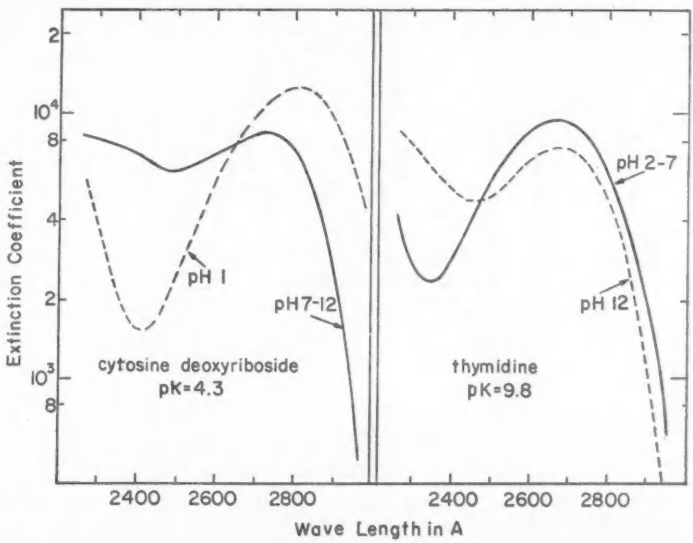

FIGURE 4 The spectra of cytosine deoxyriboside at pH 7 and 1, and the spectra of thymidine at pH 7 and 12 from reference (17). (The data at pH 1 were taken from reference 17 which reports negligible change between pH 1 and pH 2.)

creased markedly. Moreover, in agreement with the absorption spectrum at long wave lengths, the wave length of maximum sensitivity has shifted from 2600 to 2700 A. At pH 12, the UV sensitivity has increased at the lowest wave lengths, as expected qualitatively from the change in the thymidine spectrum, and is decreased significantly in the intermediate spectral range, around 2600 A. The explanation for the slightly higher sensitivity at wave lengths above 2900 A is not available. Qualitatively the changes in the action spectra parallel the changes in the absorption spectra of cytosine and thymidine. However, we would expect the changes in the action spectra to be similar to those of the absorption spectra even if the pyrimidines were not the most sensitive bases. The differences in the shapes of action and absorption spectra at pH 7 (see Fig. 2) and the *quantitative* argument given below

indicate that the pyrimidines are the important bases to consider in the absorption of light which leads to UV inactivation.

The Contributions of Pyrimidines and Purines. The relative contribution to the inactivation process of quanta absorbed in cytosine, thymine, guanine, and adenine may be found in the following way. Assume that the inactivation cross-section of the virus is the sum of the inactivation cross-sections for light absorbed in the individual bases.

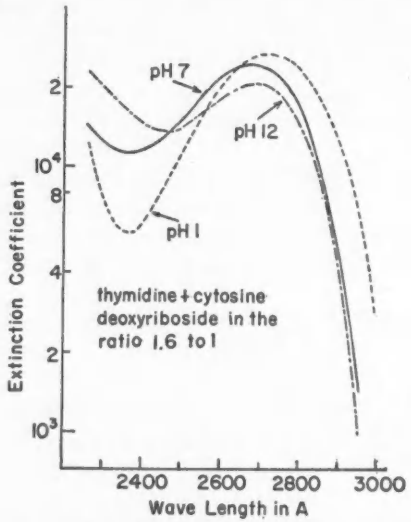

FIGURE 5 The computed absorption spectra, at pH 1, 7, and 12, of thymidine plus cytosine deoxyriboside in the molar ratio of 1.6 to 1.

$$\sigma = \sigma_C + \sigma_T + \sigma_G + \sigma_A \,. \tag{2}$$

The subscripts stands for the four bases. We use equation (1) to rewrite (2) in terms of the absorption cross-sections of the individual bases s, the number of bases n, and the quantum yield ϕ for inactivation by light absorbed in a particular type of base.

$$\sigma = \phi_C n_C s_C + \phi_T n_T s_T + \phi_G n_G s_G + \phi_A n_A s_A \,. \tag{3}$$

In so far as the absorption coefficient of the viral DNA is the sum of the coefficients of the four bases, this is a valid relation. We assume that the only parameters in equation (3) which are pH dependent are the absorption and inactivation cross-sections. If $\Delta\sigma_{7-2}$ and $\Delta\sigma_{7-12}$ represent the changes in inactivation cross-sections for the pH changes 7 to 2 and 7 to 12,

$$\Delta\sigma_{7-2} = \phi_C n_C \, \Delta s_C \,, \tag{4}$$

and

$$\Delta\sigma_{7-12} = \phi_T n_T \Delta s_T \,. \tag{5}$$

We can measure Δs_C, Δs_T, and the corresponding values of $\Delta\sigma$ and, from a knowledge of n_C and n_T we may compute ϕ_C and ϕ_T. The values of ϕ_C and ϕ_T found in this way may be substituted back into (3) so as to find $(\phi_G + \phi_A)$. Since the changes in absorption spectra of the bases inside the virus will be *less* than in solution, the values of ϕ_C and ϕ_T which we calculate will be *minimum* values.

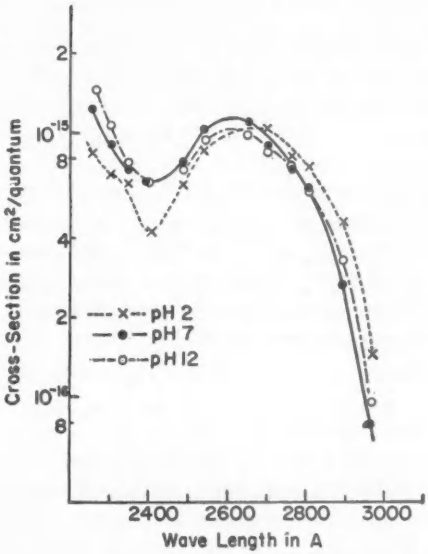

FIGURE 6 The action spectra for the inactivation of ΦX174 at pH 2, 7, and 12.

The assumption that ϕ_C *and* ϕ_T are pH-independent is verified in the following way. In changing the pH from 7 to 2 the absorption spectrum of cytosine does not change at 2650 A (see Fig. 4). If ϕ is pH-independent, this wave length should show the same inactivation cross-sections at pH 7 and 2. Actually the wave length of constant σ is 2680 A. For the change from pH 7 to 12 we would expect, from the thymidine spectrum, similar values of σ at 2470 A. The wave length of constant σ is found near 2400 A.

The numerical values that shall be substituted into equations (3, 4, 5) are obtained from Sinsheimer's (1) data on the base composition of ΦX174 and from the absorption and action spectra shown in Figs. 4 and 6. The data and derived values of ϕ_C and ϕ_T are shown in Tables I and II. The computed absorption cross-section

TABLE I

DATA USED FOR THE CALCULATION OF ΦX174 ABSORPTION AT 2650 A, pH 7

Base	No. of bases	Absorption per base	Absorption by all bases
Cytosine	970	3.2×10^{-17} cm²	3.1×10^{-14} cm²
Thymine	1550	3.7	5.7
Guanine	1250	3.8	4.8
Adenine	1230	4.6	5.6
		Sum	19.2×10^{-14}

is within 5 per cent of the observed value for viral DNA shown in Fig. 2*b*. It should be clear from an inspection of Fig. 6 that the values of $\Delta\sigma$ for thymidine, shown in Table II B, are subject to large experimental errors, perhaps as large as 50 per cent, because the changes between the action spectra at pH 7 and 12 are small. The average value for the quantum yield for the inactivation of the virus by the quanta absorbed in the two pyrimidines is 0.0085. If we assume this value is the actual value for thymine and cytosine we may use it to obtain, from equation (3), an estimate for the quantum yield for quanta absorbed in adenine and guanine. There is no practical way to determine the effects on the bases separately so we assume, in addition, that the quantum yields for inactivation by absorption in the two purines are the same and are wave length- and pH-independent. Equation (3) takes the form

$$\sigma = 0.0085(n_C s_C + n_T s_T) + \phi_{G,A}(n_G s_G + n_A s_A).$$

At pH 7 and 2650 A the value of σ, 1.1×10^{-15} cm², and the other numbers shown in Table I yield $\phi_{G,A} = 0.0034$. If similar computations, using the proper values of absorption and action cross-sections, are made at other wave lengths, we obtain at

TABLE II

DATA USED TO CALCULATE ϕ_C AND ϕ_T

A. pH 7–2

λ	Δs_C	$\Delta\sigma_{7-2}$	ϕ_C Calculated from (4)
2400 A	2×10^{-17} cm²	2.3×10^{-16} cm²	0.012
2900	3×10^{-17}	1.9×10^{-16}	0.006

B. pH 7–12

λ	Δs_T	$\Delta\sigma_{7-12}$	ϕ_T Calculated from (5)
2300 A	1.9×10^{-17} cm²	1.7×10^{-16} cm²	0.006
2650	0.8×10^{-17}	1.2×10^{-16}	0.010
		Average of ϕ_C and ϕ_T	0.0085

2480 A, $\phi_{G,A} = 0.0038$ and at 2400 A, $\phi_{G,A} = 0.0042$. The facts that the absorption spectrum of guanosine changes in the pH range 7 to 12 and that ϕ_G is not negligible do *not* affect equation (5) because the spectral changes are very small at 2300 and 2650 A. Because the value 0.0085, which represents ϕ_C and ϕ_T in the above equation, is a minimum value, the computed $\phi_{G,A}$ represents a *maximum*.

The values of $\phi_{G,A}$ are very sensitive to the value used for the quantum yield for cytosine and thymidine. If, for example, we had used a value of 0.012 for ϕ_C and ϕ_T, we would have obtained for $\phi_{G,A}$ a value of 3×10^{-4} at 2650 A. These calculations indicate that quanta absorbed in the pyrimidines have at least a 2 to 3 times greater chance of inactivating the virus than those absorbed in the purines. This result is the quantitative foundation for the statement that the action spectra for single-stranded polynucleotides should differ from double-stranded ones because in the later the non-localization of absorbed energy means that *all* absorbed quanta have equal inactivation probabilities.

Quantum yields for the spectral alteration of the free nucleotides are about the same as the numbers for affecting the bases of ΦX174. They range from 0.01 for cytosine, to about 0.0001 for the purines (3). The value for the alteration of thymidine is 0.001 but its interpretation is complicated by the fact that in solution there is a rapid reversible reaction which may not occur in the virus. A value of $\phi_{G,A}$ for the virus which is greater than values found for free bases indicates, in our method of interpretation, that the bases are really *not* completely independent and that a quantum absorbed in a purine has a non-zero probability of affecting a pyrimidine.

The alternative explanation for the shape of the action spectra, which we discarded above, namely that the spectra are the sum of action on nucleic acid and protein, does not stand up to quantitative examination. For example, the spectrum of tyrosine (18) changes drastically in going from pH 7 to 12. There is a big increase in absorption at 2900 A and a maximum absorption at 2600 A. These changes do not show up in the action spectrum of the virus. The spectral changes of tryptophan are somewhat similar to those found in the action spectra in going from pH 7 to 12, but available data on the quantum yield for an inactivation of structures by absorption of light in tryptophan (4) indicate that the quantum yield is about 0.002. This is too low an efficiency to produce the effects observed here. The spectrum of neither tyrosine nor tryptophan changes much on acidification and thus it cannot account for the observed change in the action spectrum in going from pH 7 to 2. It looks as if the only simple explanation for the action spectra for inactivation of ΦX174 is that most of the effect of the absorbed light takes place owing to quanta absorbed in the two pyrimidines and that the intrinsic sensitivity of the pyrimidines increases at short wave lengths.

If, contrary to the above analysis, the proper interpretation of the action spectra is in terms of the effect of light on nucleoprotein, one would still expect single-

stranded polynucleotides to have minima at longer wave lengths than those of double-stranded DNA. Any energy transfer or reaction between proteins, which have absorbed light between 2300 and 2400 A, and nucleic acid polymers should be more efficient with the more intimate contact between protein and single-stranded structures. This indirect mechanism may be the explanation for the shape of the action spectrum of tobacco mosaic virus (19). It is improbable that a direct effect of ultraviolet light on viral proteins would affect virus survival because, for example, in the T-even bacterial viruses the majority of the viral protein does not enter the host (20) and in the plant viruses the protein is made up of many identical subunits (21), any one of which is probably dispensable.

CONCLUSION

The action spectra for the inactivation of ΦX174 at three pH's have been analyzed in terms of contributions of the four bases—cytosine, thymine, guanine, and adenine. The action spectra all show minima at 2400 A rather than the characteristic absorption spectrum minimum of DNA at 2300 A. The action spectra, which heretofore have been interpreted in terms of the effects of light on nucleoprotein, are simpler to interpret in terms of the preferential action of light on cytosine and thymine. If this interpretation is correct, action spectra offer a convenient experimental way of distinguishing biological actions which take place *via* single- or double-stranded structures. Single-stranded structures should have action spectra minima at 2400 A; double-stranded DNA should have a minimum closer to 2300 A.

REFERENCES

1. SINSHEIMER, R. L., A single-stranded deoxyribonucleic acid from bacteriophage ΦX174, *J. Mol. Biol.*, 1959, **1**, 43.
2. ERRERA, M., Etude photochimique de l'acide desoxyribonucléique, *Biochim. et Biophysica Acta*, 1952, **8**, 30.
3. SHUGAR, D., and WIERZCHOWSKI, K. L., Photochemistry of nucleic acids, nucleic acid derivatives and related compounds, *Postepy Biochemii*, 1958, **4**, 243.
4. SETLOW, R., Action spectroscopy, *Advances Biol. Med. and Physics*, 1957, **5**, 37.
5. SETLOW, R., The use of action spectra to determine the physical state of DNA *in vivo*, *Biochim. et Biophysica Acta*, 1960, **39**, 180.
6. SETLOW, J. K., and SETLOW, R. B., Evidence for the existence of a single-stranded stage of T2 bacteriophage during replication, *Proc. Nat. Acad. Sc.*, 1960, **46**, 791.
7. ZAHLER, S. A., Some biological properties of bacteriophages S13 and ΦX174, *J. Bact.*, 1958, **75**, 310.
8. FLUKE, D. J., and SETLOW, R. B., Water-prism ultraviolet monochromators, *J. Opt. Soc. Am.*, 1953, **44**, 327.
9. MOROWITZ, H. J., Absorption effects in volume irradiation of microorganisms, *Science*, 1950, **111**, 229.
10. SINSHEIMER, R. L., The photochemistry of cytidylic acid, *Radiation Research*, 1957, **6**, 121.
11. STENT, G. S., Mating in the reproduction of bacterial viruses, *Advances Virus Research*, 1958, **5**, 95.

12. ZELLE, M. R., and HOLLAENDER, A., Monochromatic ultraviolet action spectra and quantum yields for inactivation of T1 and T2 *Escherichia coli* bacteriophages, *J. Bact.*, 1954, **68,** 210.
13. SETLOW, R., and DOYLE, B., The effect of light of wavelength 2,537 A on proteins and nucleic acid at low temperatures, *Biochim. et Biophysica Acta*, 1953, **12,** 508.
14. SHORE, V. G., and PARDEE, A. B., Energy transfer in conjugated proteins and nucleic acids, *Arch. Biochem. and Biophysics*, 1956, **62,** 355.
15. SINSHEIMER, R. L., and HASTINGS, R., A reversible photochemical alteration of uracil and uridine, *Science*, 1949, **110,** 525.
16. WANG, S. Y., Ultraviolet irradiation of 1,3-dimethylthymine, *Nature*, 1959, **184,** 59.
17. BEAVEN, G. H., HOLIDAY, E. R., and JOHNSON, E. A., Optical properties of nucleic acids and their compounds, *in* The Nucleic Acids. Chemistry and Biology, (E. Chargaff and J. N. Davidson, editors), New York, Academic Press, Inc., 1955, **1,** 493.
18. BEAVEN, G. H., and HOLIDAY, E. R., Ultraviolet absorption spectra of proteins and amino acids, *Advances Protein Chem.*, 1952, **7,** 319.
19. HOLLAENDER, A., and DUGGAR, B. M., Irradiation of plant viruses and microorganisms with monochromatic light. III. Resistance of the virus of typical tobacco mosaic and *Escherichia coli* to radiation from λ 3000 A to λ 2250 A, *Proc. Nat. Acad. Sc.*, 1936, **22,** 19.
20. HERSHEY, A. D., Bacteriophages as genetic and biochemical systems, *Advances Virus Research*, 1957, **4,** 25.
21. MARKHAM, R., The biochemistry of plant viruses, *in* The Viruses, (F. M. Burnet and W. M. Stanley, editors), New York, Academic Press, Inc., 1959, **2,** 33.

PHYSICAL STUDIES ON POX VIRUSES

I. Inactivation of Vaccinia Virus Infectivity with Low-Energy Electrons

J. F. McCrea, John W. Preiss, *and* Jean O'Loughlin
From the Department of Biophysics, Yale University, New Haven. Dr. Preiss's present address is Laboratory of Physical Biology, National Institute of Arthritis and Metabolic Diseases, Bethesda

ABSTRACT Vaccinia virus was irradiated *in vacuo* with low-voltage electrons of restricted ranges. It was found that the pock-forming ability of the virus was not decreased after bombardment with electrons penetrating 100 A beneath the virus surface. There was very slight reduction in titer with large doses of electrons penetrating 330 A, but a sudden marked drop in infectivity occurred after exposure to electrons penetrating 500 to 700 A. Electrons of higher energies, including those capable of penetrating the virus particle completely, did not produce significant further fall in infectivity titer. It is concluded that a highly radiation-sensitive unit essential for pock formation is situated 500 to 700 A beneath the surface of the virus particle, possibly in the form of a shell. The relation of this finding to the known structure of the virus and to other radiation data on the dimensions of the infectious unit is discussed.

INTRODUCTION

Vaccinia was the first animal virus inactivated with ionizing radiations. Exponential loss of infectivity following exposure to x-rays was demonstrated in 1939 by Gowan and Lucas (1), and similar inactivation curves were obtained shortly afterwards by Lea and Salaman (2) in more detailed experiments with x-rays, gamma rays, and alpha particles. The virus has been studied recently with high-energy ionizing particles from several radiation sources, and from the slope of the inactivation curves so obtained it has been concluded that the infectious unit may be represented as a sphere approximately 500 A in diameter (3).

In this paper we describe experiments in which dry vaccinia virus was exposed to low-energy electrons of restricted ranges; *i.e.*, electrons accelerated to velocities sufficient to penetrate to predetermined depths. Such particles have previously been

This work was supported by grant E 2213 of the United States Public Health Service.
Received for publication, May 26, 1960.

used to study the intracellular distribution of enzymes in yeast (4, 5), and also to investigate structures within bacterial spores (6, 7). The T_1 bacteriophage (8) and Newcastle disease virus (9) have been shown to possess radiation-insensitive "skins" 200 to 500 A thick by means of low-energy electron bombardment.

Because of its large size and because of the complex structures apparent in thin sections of the virus particle examined with the electron microscope (16, 17), vaccinia virus seemed particularly suitable for "partial virus irradiation" with low-energy electrons, with the aim of discovering which zone, if any, was particularly associated with the property of infection and consequent pock formation. It also seemed valuable to compare such results to those obtained from inactivation of infectivity with high-energy electrons and other particles. A preliminary account of some of these experiments was included in a general review of the effects of ionizing radiations on animal viruses (3).

MATERIALS AND METHODS

Bombardment. The accelerator used in all these experiments has been described previously (4). In essence the machine consists of a vacuum chamber 28 inches in diameter, in which stainless steel discs (½ inch diameter) covered with material to be irradiated are arranged in concentric rings; electron guns rotating above the discs deliver a homogeneous electron beam which is recorded by a galvanometer. Dose is determined by the number of revolutions of the electron guns over the target. At least ten discs were used for each assay point, and groups of controls were placed in the vacuum chamber, but out of range of the electron beam, in each experiment.

Virus Preparation. The Levaditi strain of vaccinia virus, which had been through at least 15 consecutive passages on the chorioallantoic membrane of 12-day chick embryos, was used throughout. Embryos were inoculated with 0.1 ml of virus diluted 10^{-3} to 10^{-4}, and the membranes removed after incubation at 37° for 48 hours. Membranes showing semiconfluent pocks were cut finely with scissors and then homogenized thoroughly with glass TenBroeck homogenizers, allowing 1 ml of normal saline buffered with M/100 pH 7.1 phosphate buffer for each membrane. Aliquots of the homogenate were frozen at −20° in small sealed tubes, and thawed and centrifuged at slow speed immediately before use.

In preliminary experiments, infectious particles were deposited from the membrane homogenate by centrifugation for 1 hour at 30,000 *g*, washed once with distilled water, and resuspended in the original volume of distilled water. All these procedures were carried out at 4°C. The virus shows little or no significant loss in infectivity after exposure to distilled water, as observed previously by Hoagland, Smadel, and Rivers (10), and is in fact resistant to inactivation by osmotic shock from 10 per cent NaCl into distilled water (11). However, freeze-drying of the washed virus on stainless steel discs by various methods gave highly irregular and unpredictable infectivity titers, and on occasion the titer dropped 2 to 3 logs. Similar difficulty was experienced with dry Newcastle disease virus on stainless steel (9). In spite of variations in freezing and drying techniques, we were unable to obtain consistent high-titer dried virus after centrifugation and washing in distilled water. Since it seemed important to irradiate virus which was as undamaged as possible by preliminary treatment, further experiments were performed in

which virus-containing homogenate was dialyzed against distilled water at 4° overnight, diluted 10^{-2} in distilled water, and then lyophilized on steel discs. Loss of infectivity was slight after these procedures, being at most 50 per cent of the untreated virus titer, and in the majority of experiments considerably less. Although such dried virus is undoubtedly contaminated with materials from the host tissue, the inactivation curves obtained below suggest that the contamination was without significant effect.

The exact procedure finally adopted was as follows: Infected membranes were washed and homogenized in distilled water, diluted 10^{-2} or 10^{-3} in distilled water, and 0.02 ml volumes pipetted onto scrupulously clean stainless steel discs. The virus was frozen on the discs at −20°, and then transferred to a chilled desiccator which was connected to a high vacuum pump for 2 to 3 hours. When dry, the virus suspension formed a uniform, barely visible opalescent film over the entire disc surface; granular or irregular patches over the surface were usually due to improperly cleaned discs. Such discs were discarded. When drying was complete, the discs were rapidly transferred to the irradiation chamber, which was then evacuated. After irradiation the discs were removed and each group of ten immersed in 2 ml of buffered pH 7.1 saline containing 1000 units of penicillin and 0.1 mg of streptomycin/ml. The tubes containing the discs were allowed to stand for 20 minutes at 4° with occasional shaking. The resuspended virus was then diluted in 10-fold steps, and 0.1 ml volumes rapidly inoculated into groups of at least six 12-day chick embryos for each dilution. Pock counts were made after incubation at 37° for 48 hours, the end point being taken at the dilutions which showed an average of 20 to 30 pocks per membrane (12). With careful standardization of all steps described, the titer of resuspended control virus was remarkably uniform in all experiments, the range of activity being from 2×10^7 to 8×10^7 pock-forming units (PFU) per ml.

RESULTS

Dose-survival curves for vaccinia virus irradiated with electrons of six different energies are shown in Figs. 1 to 4. In each experiment virus activity is plotted as per cent of the titer of controls which were shielded from the electron beam but otherwise treated identically. Different symbols on each curve represent data from different experiments.

Fig. 1 shows that no decrease in infectivity occurs after exposure to 500 volt electrons, even at the highest doses (16×10^{13} electrons/cm^2). Further experiments are required to show whether or not the slight upward curvature is statistically significant. A similar "activating" effect has been observed when this virus was exposed to low doses of electrons in other types of accelerators (11). One thousand volt electrons (Fig. 2) cause considerable scatter in the data, with a possible loss of infectivity at the highest electron dose.

The inactivation curve obtained after exposure to 1500 volt electrons (Fig. 3) shows an immediate drop in infectivity, at first exponential with dose, but then flattening at approximately 10 per cent of the control titer. Essentially similar curves are obtained with 2000 and 2500 volt electrons (Figs. 3 and 4). Only 4×10^{13} electrons/cm^2 are required to reduce survival to approximately 2 per cent of the controls when the electrons are accelerated by a 5000 volt field (Fig. 4).

The electron ranges given in Table I are approximately the average between those obtained experimentally by Davis (13) and those calculated by Lea (14). The former author has discussed the question of electron ranges in biological material in considerable detail (7, 8, 13), as has also Preiss (4, 5). Admittedly such ranges are not known precisely, but the reader who consults the above references will see that the agreement between experiment and theory is quite good. In most of the experiments involving such range-restricting techniques it has been the *form* of the property survival-electron energy (and therefore range) function which has been of primary importance.

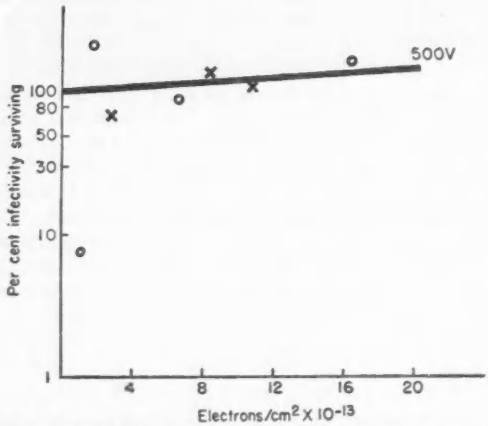

FIGURE 1 Effect of irradiating vaccinia virus with 500 volt electrons (penetration to 100 A).

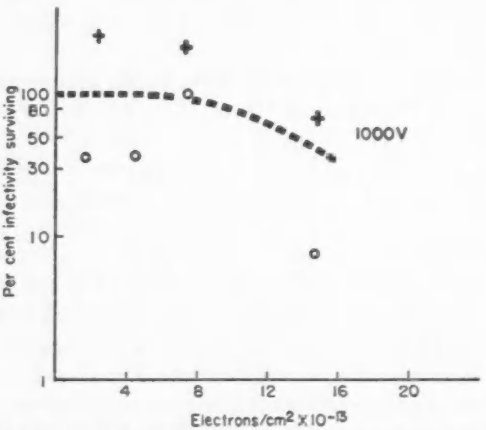

FIGURE 2 Effect of irradiating vaccinia virus with 1000 volt electrons (penetration to 330 A).

DISCUSSION

The property under study is clearly a step function of electron energy, for a sharp downward break to about 10 per cent survival occurs at 1500 volts. When a beam of mono-energetic particles is stopped in an absorbing material, there can be only an average trajectory length, for they do not all experience the exact same number of inelastic collisions while traversing a given mass of absorber. This phenomenon is called "straggling" (5), and is one of the factors which guarantees that the above mentioned step can never be a perfect discontinuity. Another more serious factor is the position of the virus particles on the bombardment discs, both relative to one another and contaminating material. In fact it could be argued that the lower-energy electrons produce no inactivation because they cannot penetrate a layer of chorioallantoic membrane and salt residues which shields the virus particles. This layer

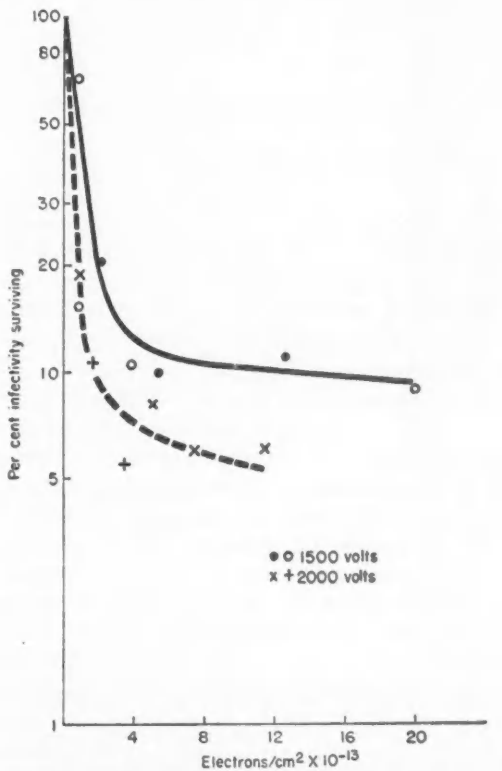

FIGURE 3 Effect of irradiating vaccinia virus with 1500 volt electrons (penetration to 700 A) and 2000 volt electrons (penetration to 1200 A).

would have to be both omnipresent and uniform, for a threshold energy exists for its penetration. It could only satisfy both of these requirements by being attached to every virus particle, for all survive 500 volt electron bombardment. On the other hand, if a conglomerate mass of virus particles and contaminating materials was on the irradiation discs, we would not expect to see the near discontinuity in the survival-electron energy function. Now the only entities on the discs which we can be sure have uniform structures are the virus particles themselves. From these considerations it is reasonable to conclude that (*a*) all virus particles have a shielding

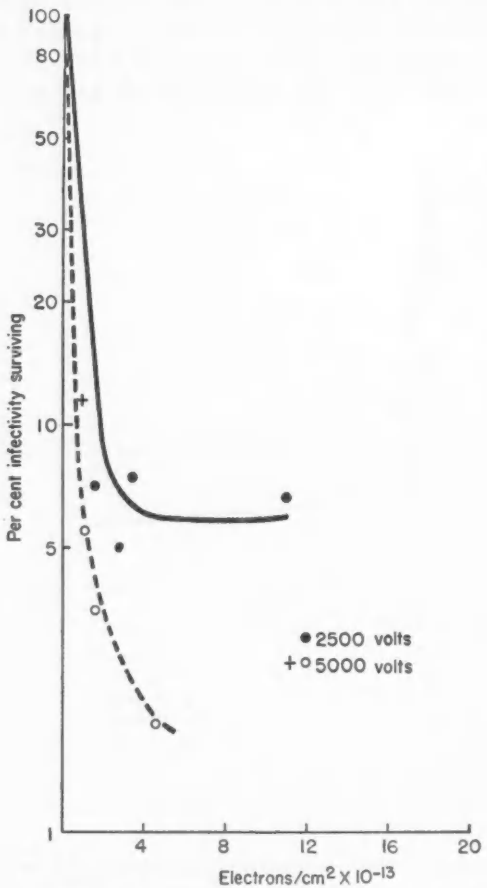

FIGURE 4 Effect of irradiating vaccinia virus with 2500 volt electrons (penetration to 1750 A) and 5000 volt electrons (penetration to 5700 A).

TABLE I

THE MEAN RANGE OF ELECTRONS IN ORGANIC MATERIAL

These are the averages of those obtained experimentally by Davis(13) and those calculated by Lea(14). Above 2000 volts they are essentially those of Lea, at density 1.3.

Energy	Range
ev	*A*
500	100
1000	330
1500	700
2000	1200
2500	1750
3000	2400
4000	3900
5000	5700

coat; (*b*) this coat is of the same thickness for all virus particles; (*c*) this coat is an integral part of the structure of a virus particle.

The 10 per cent activity remaining after bombardment with 1500 volt electrons, and approximately 6 per cent remaining after the same treatment with 2000 to 2500 volts, probably represent that portion of virus shielded by other virus particles, salt, or other contaminating substances from the membrane suspensions. The 5000 volt electrons which can easily traverse two overlapping virus particles eliminate most of this remaining activity. The faint inactivation produced by 1000 volt electrons is probably the result of straggling of electrons beyond the mean range (about 300 to 330A), since enormous doses are required to see it.

The data presented show clearly that ionizations from high doses of electrons hitting the surface of dry vaccinia particles, or penetrating as far as 330 A below the virus surface, cause little or no change in the ability of the virus to form pocks on the chorioallantoic membrane. Ionizations occurring 500 to 700 A or more beneath the virus surface, however, cause rapid and significance loss of infectivity. These results suggest that the virus possesses a relatively radiation-insensitive "skin" approximately 500 to 700 A thick, beneath which is situated a highly radiation-sensitive infectious unit.

The data from all experiments are summarized in Fig. 5, in which the inactivation curve is plotted on an arithmetic scale; beneath this curve is a schematic section of a vaccinia virus particle drawn on the same scale. The inactivation curve shows that maximum loss of infectivity occurs when electrons penetrate 500 to 700

A beneath the virus surface, and that deeper penetration (including those electrons capable of traversing the whole particle) produces no further significant fall in infectivity. That inactivation is most rapid and extensive over the electron penetration range between 330 and 750 A, and does not increase significantly with electrons ionizing deeper in the nucleoid region, suggests that an ionization on the outer edge

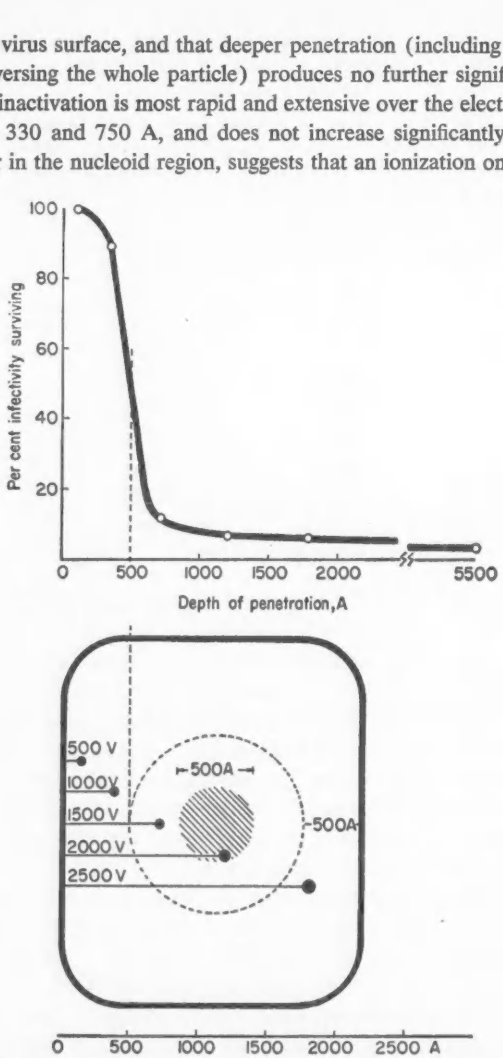

FIGURE 5 Inactivation of vaccinia virus infectivity plotted as a function of depth of electron penetration. The curve is drawn above a schematic outline of vaccinia particle on the same scale; the depth to which electrons of various voltages penetrate is indicated schematically. It should be noted that ionizations occur at random along the electron paths, and that the paths themselves are in practice not perfectly straight. The central cross-hatched circle represents the dimensions of the radiation-sensitive infectious unit calculated from bombardment with fast particles. For details see text.

of the infectious unit is capable of inactivating the whole unit. Previous inactivation experiments with high-energy ionizing particles have also indicated that a single ionization anywhere within a viral infectious unit may inactivate the whole unit (2, 14, 15). From the present experiments the outer bound of this unit is perhaps best defined from the mid-point of the steep slope of the inactivation curve, as illustrated in Fig. 5, and would thus be approximately 500 A beneath the surface, as represented by the dotted circle. Slow-electron data alone do not in this case allow one to distinguish whether the radiation-sensitive zone is in the form of a shell, or represents the outer bound of a solid core.

Irradiation of the same strain of vaccinia *in vacuo* with high-energy electrons from a Van de Graaff generator, or with gamma rays from a cobalt-60 source, gave exponential loss of infectivity down to approximately 1 per cent of the control titer. From the slope of these curves it has been calculated that the volume of the radiation-sensitive infectious units is 6.7×10^{-17} cc, which is equivalent to a sphere of approximately 500 A diameter (3). If such a sphere was located in the center of a dry vaccinia particle (2600 x 2200 A) the electrons would have to travel at least 850 A to reach the outer boundary of the sensitive region (Fig. 5). This distance, calculated from target theory (14, 15) and the geometry of the virus particle, is thus greater than that indicated by the experimental results obtained in this paper showing rapid inactivation by slow electrons penetrating 500 to 750 A beneath the virus surface. A centrally located sphere, 500 A below the virus surface, would be 1100 A in diameter, and would thus contain approximately 10 times the volume of the radiosensitive infectious unit calculated from inactivation with high-energy particles (3). This difference in the volume calculations would suggest that the radiosensitive material may be in the form of a shell, 6.7×10^{-17} cc in volume, the outer bound of which is approximately 500 A beneath the virus surface. It should be noted however, that the estimates of the electron ranges used in our experiments were originally made for proteins, and that the ranges in the outer virus coat composed of unknown proportions of proteins and lipoproteins may be slightly different.

One of the main interests in using range-restricted electrons with a virus of the complexity of vaccinia is in correlating results with the structures seen in preparations of the virus examined in the electron microscope. It has been demonstrated in electron micrographs that vaccinia contains a "nucleoid," which is susceptible to desoxyribonuclease after suitable preliminary treatments (16). Recently, Epstein (17) obtained excellent electron micrographs of ultrathin sections of vaccinia purified with a fluorocarbon, showing that the nucleoid consists of a central electron-dense discoid body and an outer region of low electron density, the whole surrounded by double membranes. Essentially similar pictures of vaccinia purified with fluorocarbon and sectioned in our laboratory show that the distance between the outer viral membrane and the double membrane surrounding the nucleoid is 350 to 400 A. At present it would be rash to draw too close comparisons between this dis-

tance and the schematic outline of the virus based on radiation experiments with slow electrons (Fig. 5), but it may be observed that the concept of virus structure obtained by two entirely different techniques is not dissimilar.

The infection of a host cell by a virus, as measured by the subsequent development of specific lesions, is a complex process dependent on several successive stages. Theoretically it should be possible to prevent the development of lesions by suitable blockade at any one of these stages. For example, the surface of the virus particle may be modified in such a way that it is unable to atach to or enter the host cell. The extremely rapid and marked loss of infectivity, concomitant with distortion of the virus surface, which follows momentary contact of vaccinia virus with concentrated urea or guanidine hydrochloride probably represents this type of inactivation (18, 19). It is extremely unlikely, however, that changes in the virus surface or outer "skin" are implicated in the present experiments, because ionizations from heavy doses of electrons penetrating up to 330 A did not significantly reduce pock-forming ability. It might be argued that since one side of all virus particles was fixed to the steel discs, and hence could be reached only by electrons penerating through at least 2200 A of virus body, all particles (except those bombarded with electrons in the 3000 to 5000 volt range) would have approximately 20 per cent of their surface untouched by electrons, and that this intact portion of the surface could be sufficient to initiate infection. Inspection of the inactivation curve in Fig. 5, however, makes this explanation extremely unlikely because there is clearly no further significant reduction in infectivity with the higher voltage electrons which are capable of penetrating through the under surface of the virus particles.

It would seem that low-voltage electrons are a useful tool in the study of large viruses such as vaccinia. Further experiments are planned to investigate surface structures such as antigens and hemagglutinins of vaccinia and other pox viruses.

The authors are indebted to Dr. E. C. Pollard for advice and interest, and to Mr. David Miles for some of the irradiations. The assistance of Miss Sigrid Angerer with electron microscopy is gratefully acknowledged.

BIBLIOGRAPHY

1. Gowen, J. W., and Lucas, A. M., Reaction of variola vaccine virus to roentgen rays, *Science*, 1939, **90**, 621.
2. Lea, D. E., and Salaman, M. H., The inactivation of vaccinia virus by radiations, *Brit. J. Exp. Path.*, 1942, **23**, 27.
3. McCrea, J. F., Ionizing radiation and its effects on animal viruses, *Ann. New York Acad. Sc.*, 1960, **83**, 692.
4. Preiss, J. W., The localization of invertase in the yeast cell with low-voltage electrons, *Arch. Biochem. and Biophysics*, 1958, **75**, 186.
5. Preiss, J. W., The effects of range-restricted electrons on intracellular yeast catalase, *Arch. Biochem. and Biophysics*, 1959, **79**, 261.
6. Knauss, H. P., Penetration of slow electrons through spore walls of *Bacillus megaterium*, *Science*, 1954, **124**, 182.

7. DAVIS, M., The irradiation of bacterial spores with low-voltage electrons, *Arch. Biochem. and Biophysics*, 1954, **48**, 469.
8. DAVIS, M., Irradiation of T-1 bacteriophage with low-voltage electrons, *Arch. Biochem. and Biophysics*, 1954, **49**, 417.
9. WILSON, D., and POLLARD, E. C., Radiation studies on the infective property of Newcastle disease virus, *Radiation Research*, 1958, **8**, 131.
10. HOAGLAND, C. L., SMADEL, J. E., and RIVERS, T. M., Constituents of elementary bodies of vaccinia, *J. Exp. Med.*, 1940, **71**, 737.
11. MCCREA, J. F., and O'LOUGHLIN, J., unpublished results, 1959.
12. OVERMAN, J. R., and TAMM, I., Quantitative titration of vaccinia virus on the chorioallantoic membrane, *J. Immunol.*, 1956, **76**, 228.
13. DAVIS, M., Range measurements of low voltage electrons, *Physical Rev.*, 1954, **94**, 243.
14. LEA, D. E., The action of Radiation on Living Cells, Cambridge University Press, 1947.
15. POLLARD, E. C., The Physics of Viruses, New York, Academic Press, Inc., 1953.
16. PETERS, O., Morphology of resting vaccinia virus, *Nature*, 1956, **178**, 1453.
17. EPSTEIN, M. A., An investigation of the purifying effect of a fluorocarbon on vaccinia virus, *Brit. J. Exp. Path.*, 1958, **39**, 436.
18. MCCREA, J. F., and O'LOUGHLIN, J., Effect of concentrated urea solutions on the infectivity and haemagglutinin of vaccinia virus, *Nature*, 1959, **184**, 1497.
19. MCCREA, J. F., ANGERER, S., and O'LOUGHLIN, J., Electron microscope and infectivity studies on vaccinia virus treated with urea, guanidine-hydrochloride, and sodium desoxycholate, *Bact. Proc.*, 1960, 125.

THE STRUCTURE OF TOBACCO MOSAIC VIRUS AND ITS COMPONENTS: ULTRAVIOLET OPTICAL ROTATORY DISPERSION

NORMAN S. SIMMONS *and* ELKAN R. BLOUT

From The Laboratory of the Children's Cancer Research Foundation and Harvard Medical School, Boston, and The Department of Biophysics and Nuclear Medicine, Laboratory of Nuclear Medicine and Radiation Biology, The University of California, Los Angeles School of Medicine, Los Angeles. Dr. Blout's alternate address is Research Division, Polaroid Corporation, Cambridge, Massachusetts

ABSTRACT An investigation has been made of the optical rotatory dispersion in the region 226 to 366 mμ of tobacco mosaic virus (TMV), the protein subunits isolated therefrom, the rods synthesized from the protein subunits, and the ribonucleic acid (RNA) isolated from TMV. Both TMV and the protein rods show anomalous rotatory dispersion. The RNA shows a Cotton effect with an inflection point around 260 mμ, which is shifted to 272 mμ in concentrated urea solution. A suggested interpretation of the RNA rotatory dispersion is given. The rotatory dispersion of the protein subunits shows an incipient Cotton effect with an inflection point around 293 mμ and the beginnings of a large negative Cotton effect with a trough at 232 mμ. The dispersion data from the protein subunits can be interpreted to indicate that they contain between 25 and 35 per cent α-helix. On the basis of recent sequence investigations and the relationship between amino acid composition and polypeptide structure, the helical portion of the protein subunits can be located in the central section of the protein chain.

INTRODUCTION

As a result of extensive x-ray diffraction, chemical, and physical-chemical studies, tobacco mosaic virus (TMV) has been shown to be a hollow cylinder of helically arranged asymmetric protein subunits containing within them a single ribonucleic acid (RNA) chain which winds between turns of the protein helix. A complete review of the known structural parameters of TMV has recently been prepared by Klug and Caspar (1).

This work was supported in part by United States Public Health Service Grant A2558 and by Contract No. AT(04-1)-GEN-12, between the Atomic Energy Commission and the University of California.

Received for publication, August 15, 1960.

The protein subunits may be isolated free of RNA (2) and reversibly aggregated into hollow, cylindrical rods as a function of temperature, pH, and ionic strength (3). X-ray diffraction studies indicate that these RNA-free protein rods have an internal structure almost indistinguishable from that of the protein shell of the original virus (4).

X-ray diffraction and birefringence studies have indicated the RNA chain to be coiled between turns of the helical protein shell and the planes of the purine and pyrimidine bases aligned approximately parallel to the fiber axis of the virus (5). Since the pitch of the virus helix is 23 A, there is no possibility of hydrogen bonding between bases on successive turns of the helix and the structure of the RNA in the TMV will collapse when the protein is removed. Thus any secondary structure of isolated RNA must be due to base interactions that do not exist in the RNA contained in the virus. The fact that there is secondary structure in isolated TMV-RNA is indicated by ultraviolet absorption spectra and visible optical rotation measurements (6, 7).

The amino acid composition of the protein subunit has been known for some time and the sequence of these amino acids has been recently determined (8), but there is little information available as to the structure or conformation of the protein chain itself (9, 10). The most direct evidence on the structure of the protein subunit is that obtained from studies of the infrared dichroism of oriented TMV. These studies (9, 10) indicate that the protein subunits contain α-helices oriented radially to the long axis of the tobacco mosaic virus.

Since it is now possible to characterize certain asymmetric macromolecular structures by optical rotatory dispersion we have determined the dispersion characteristics of the whole virus, the RNA-free repolymerized protein rods, and the individual protein subunits as well as the isolated RNA. This paper presents the data which show (*a*) that the "native" TMV-protein subunits have in themselves a characteristic optical rotatory dispersion indicating a considerable helix content; (*b*) that this characteristic dispersion is altered markedly by polymerization of the subunits into protein rods—a "superhelix"; (*c*) that the isolated RNA shows rotatory dispersion with a Cotton effect having an inflection point at about 260 mμ, the significance of which will be discussed below.

EXPERIMENTAL

Materials

Tobacco Mosaic Virus (TMV). Leaves of *Nicotiana tabacum* var. *Turkish Samsun,* infected with the U_1 strain (11), were harvested and frozen. The partially thawed leaves were homogenized with distilled water and deionized with a mixture of weak base resin (amberlite CG-45) and weak acid resin (amberlite CG-50). The pulp and resin were removed from the extract by centrifugation and the supernate made 0.01 M with versene at pH 7.3. The virus was isolated by differential centrifugation (12) from 0.01 M

versene three times. The clear colorless virus pellet was finally taken up in water to a concentration of 2 per cent and dialyzed to remove residual salt.

TMV-PROTEIN SUBUNITS. The protein subunits of TMV were isolated with minor improvisations according to the method of Fraenkel-Conrat (2) using cold 66 per cent acetic acid. Ultracentrifugal analysis showed the protein to have a sedimentation constant of 4 and to be essentially homogeneous.

FORMATION OF PROTEIN RODS. The protein rods were formed from the protein subunits of TMV by the addition of NaH_2PO_4 to a concentration of 0.01 M. On ultracentrifugal analysis these rods showed a hypersharp peak with a sedimentation constant of about 200, remarkably similar to the original whole virus. Also, x-ray diffraction showed these synthesized rods to be essentially similar in internal structure to the whole tobacco mosaic virus with the exception, of course, of the absence of the RNA (13).

PREPARATION OF THE TMV-RIBOSE NUCLEIC ACID (TMV-RNA). The RNA was isolated from the virus after the method of Cohen and Stanley (14). 5 ml of 0.10 per cent TMV in 0.1M phosphate buffer, pH 7.2, was rapidly pipetted into a 13 x 150 mm test tube (containing a quarter-inch teflon-covered magnetic stirring bar) immersed in a water bath maintained at 80° over a magnetic stirrer hot plate. The solution became turbid with coagulated denatured protein in about 45 seconds. After a total of 60 seconds the tube was removed from the bath and immediately plunged directly into an ice bath similarly mounted on another magnetic stirrer. Coagulated protein was removed by centrifugation at 7,000 R.P.M. in a Servall at 4°. The water-clear supernate showed a typical ultraviolet RNA spectrum with a maximum at 259 mμ and a minimum at 230 mμ, indicating almost complete absence of contaminating protein. The yield was almost invariably 100 per cent of the RNA contained in the virus.

DENATURED PROTEIN SUBUNITS AND RNA. Aliquots of the protein subunits and RNA were made 8 M with recrystallized urea and held at 60° for 1 hour and then cooled to room temperature. All further dilutions for rotation measurements were made with 8 M urea. The 8 M urea solutions themselves showed no rotation.

Method

Optical rotations were measured with a Rudolph photoelectric polarimeter, model 200 using a General Electric AH-6 water-cooled high pressure mercury arc as the light source. The lamps were selected for maximum output below 240 mμ. A Beckman DU monochromator was used to obtain essentially monochromatic radiation. Since the measurements were made in the region from 366 mμ down into the far ultraviolet the quartz lens that focuses the lamp into the monochromator was adjusted so as to achieve maximum light intensity at 297 mμ. All solutions were measured in fused quartz cells of 1 cm path length selected to have minimum birefringence. All measurements were made at a symmetrical angle of 5°. Because of the high absorbance of these solutions in this wavelength region it was necessary to make careful adjustments of solute concentrations to get maximum rotation readings consistent with their absorbance characteristics. This meant taking a set of measurements for a given solute concentration over a small spectral increment.

The data are expressed in terms of specific rotation which is defined as $[\alpha]_\lambda^t = 100\alpha/l \cdot c$, where α = the observed rotation in degrees, and c = the concentration of the solute in grams per 100 ml solution and l = cell path (in decimeters). Because of the high absorbance and the necessity for working with dilute solutions, the measured rotations were very small and frequently below 0.1°. We estimate that our maximum uncertainty

for a reading at a particular wavelength in these regions is ±0.01° with an internal constancy of ±0.005°.

RESULTS AND DISCUSSION

TMV-PROTEIN SUBUNITS. The rotatory dispersion data of the protein subunits over the wavelength range 226 to 366 mμ are shown in Fig. 1. It is apparent that this protein shows anomalous rotatory dispersion and therefore the data do not fit

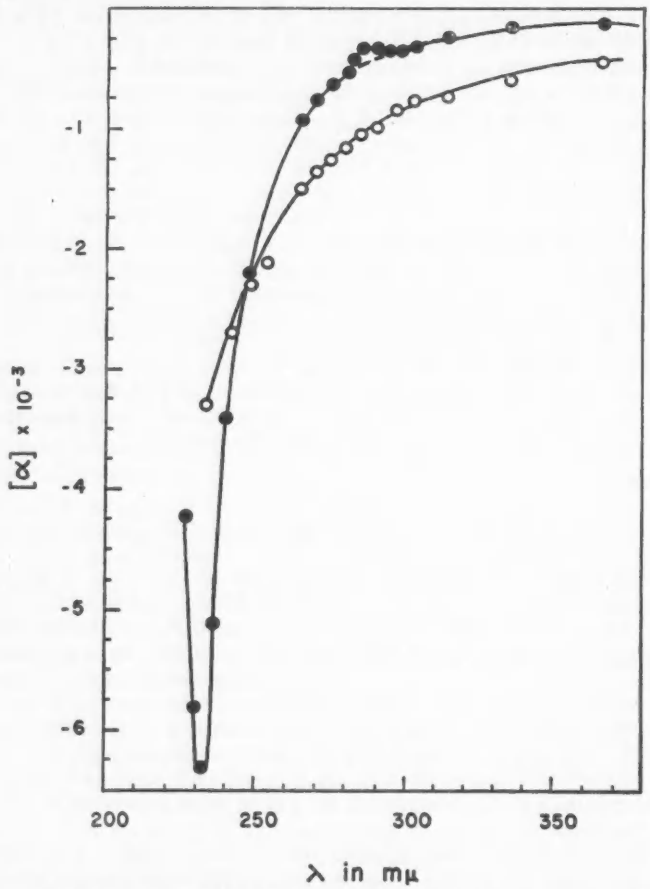

FIGURE 1 ●-●-●-●-, the rotatory dispersion of protein subunits from tobacco mosaic virus in distilled water, o-o-o-o-, the denatured form of the protein subunits of tobacco mosaic virus in 8 M urea solution.

a simple Drude equation. Over the wavelength region 365 to 600 mμ the rotation data do fit the two term relation suggested by Moffitt (15) and from this relation the coefficient of the second term b_0 has been calculated to be equal to −160. Assuming that fully α-helical polypeptides and fibrous proteins have b_0 values about 600 (16) then, on this basis, it appears that the protein subunits of TMV contain about 25 per cent α-helix.

Another indication that the protein subunits contain a helix is the fact that the beginning of an ultraviolet Cotton effect is observed with a trough at 233 mμ. This Cotton effect has recently been found to be characteristic of the α-helical form of certain synthetic polypeptides and fibrous proteins (17). When the protein subunits are denatured this ultraviolet Cotton effect is lost (Fig. 1). Furthermore it should be noted that the amino acid sequence analysis (8) indicates that both terminal positions of the protein chain contain large sequences of non-helix-forming amino acid residues (18). Thus it is clear that the helical part of the protein chain resides in the central portion.

One additional feature of the rotatory data of the native protein subunits is the presence of a small inflection point—perhaps an incipient Cotton effect—around 293 mμ. This is the first such effect observed for a native protein but detailed investigation of it will require improved instrumentation. The region around 280 to 290 mμ is where such a Cotton effect would be observed if oriented aromatic amino acids exist in the TMV-protein subunits. It is possible that this effect can be assigned to oriented tryptophan or phenylalanine residues since oriented tyrosyl groups show a Cotton effect at shorter wavelengths (19).

PROTEIN RODS. When the protein subunits of TMV are polymerized to form helical protein rods, the optical rotation changes to more positive values and there is essentially no rotation above 270 mμ (Fig. 2). This change in rotatory dispersion, a consequence of the formation of the helical rods, cannot be precisely interpreted at this time.

TOBACCO MOSAIC VIRUS (TMV). The rotatory dispersion of native TMV over the wavelength range 230 to 366 mμ is shown in Fig. 2. The data indicate that the dispersion is anomalous (in that the rotation changes from positive to negative). The reason for this anomalous dispersion of course lies in the asymmetry of the virus structure. Since the rotatory dispersion of TMV is quite different from that of the TMV-protein rods, the assumption is that this difference is due to the RNA moiety.

It is noted, however, that the TMV itself shows strongly positive rotation above 275 mμ with a maximum at approximately 285 mμ. This strong positive contribution must be assigned to the presence of the RNA helix in the intact virus. Detailed examination of the dispersion curves of the TMV and the TMV-protein rods from 270 to 236 mμ may, therefore, similarly be interpreted as being due to the presence of the RNA in the intact TMV. If a mathematical subtraction of the TMV-protein

rod dispersion data from those of the intact TMV is performed, a calculated dispersion curve attributable to the RNA, shown in the dashed line in Figs. 2 and 3, is obtained.

ISOLATED TMV-RNA. In Fig. 3 the rotatory dispersion of TMV-RNA can be seen to be anomalous and in fact shows a Cotton effect at 260 mμ, the region of absorption of the component purine and pyrimidine bases.

The presence of a Cotton effect with its inflection point at the absorption maximum of the component bases indicates that these bases are involved in an asymmetric conformation. To ascertain whether the magnitude and position of the Cotton effect reflect interaction between oriented H-bonded purines and pyrimidines, or are due only to the asymmetric environment around the optically active ribose moiety, we have attempted to disrupt any such bonding by treatment with 8 M urea. The data are shown in Fig. 3 where it can indeed be seen that there is a marked change in the dispersion curve obtained in urea solution as compared with same

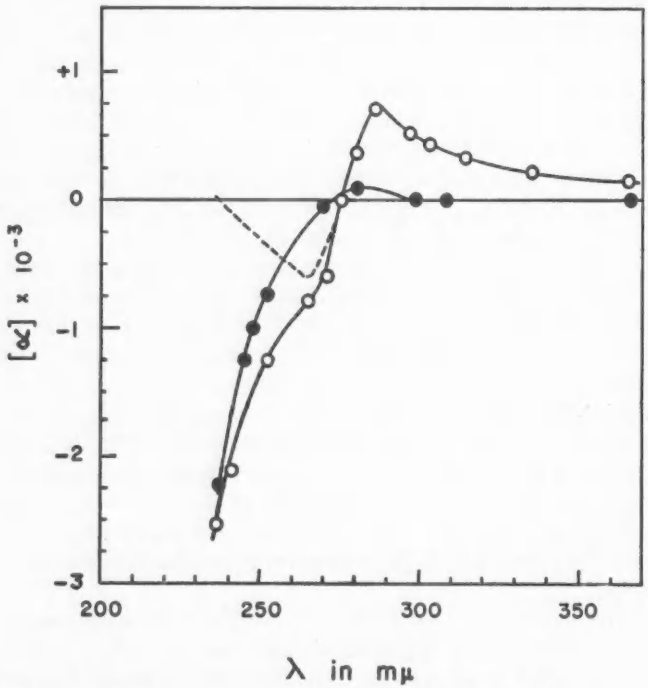

FIGURE 2 o-o-o-o-, the rotatory dispersion of tobacco mosaic virus in distilled water. •-•-•-•-, the rotatory dispersion of the protein rods synthesized from the tobacco mosaic virus-protein subunits in 0.01 M NaH_2PO_4. - - - -, the calculated curve obtained by subtracting the rotatory dispersion of the protein rods from that of the tobacco mosaic virus.

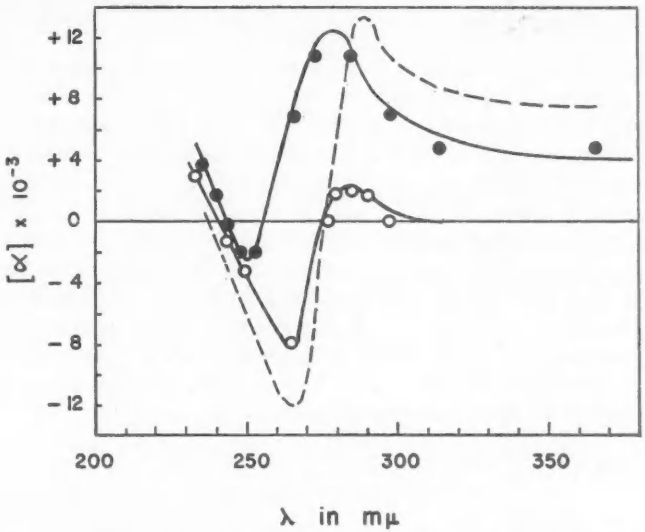

FIGURE 3 ●-●-●-●-, the rotatory dispersion of ribonucleic acid in phosphate buffer isolated from TMV as described in the experimental section. o-o-o-o-, the rotatory dispersion of ribonucleic acid from tobacco mosaic virus in 8 M urea. ----, the calculated curve (multiplied by 20 because the RNA content of TMV ≃ 5 per cent) obtained by subtracting the rotatory dispersion of the protein rods from that of the tobacco mosaic virus.

material in water. The curve has been shifted toward longer wavelengths with a concomitant diminution of the positive rotatory portion. Exciton theory (15, 20) indicates that a shift toward longer wavelengths results from the disruption of (intramolecular hydrogen bonding between) card-stacked chromophores whereas a shift towards shorter wavelengths results from disruptions of end-to-end-bonded chromophores. We thus conclude that there may be some planar (card-stacked) base-to-base interaction in isolated RNA in water solution.

It is important to note that the "calculated" RNA rotatory dispersion curve shows approximately the same inflection point (270 to 275 mμ) as the urea-treated RNA. Thus the rotatory dispersion data on RNA can be interpreted as indicating the lack of planar base-base bonding of the RNA in the native TMV in agreement with the conclusions from x-ray studies, and the presence of base-base interaction in isolated RNA in water solution. The magnitude of the "calculated" RNA dispersion curve suggests that the bases are indeed rigidly oriented in TMV as suggested by the strong positive birefringence. Taken as a whole the physical-chemical evidence indicates that in TMV the RNA exists in a rigid structure which might involve bonding of the base to sites on the protein shell or through the medium of bound water.

CONCLUSIONS

The most important conclusion from the optical rotatory dispersion data is that the helix content of the protein subunits can be estimated as being between 25 and 35 per cent. This estimate of helix content is based on both visible and ultraviolet optical rotatory dispersions. Although the rotatory dispersion changes markedly when the protein subunits are polymerized into protein rods, no interpretation of these data can be made at this time. However, from the optical rotatory dispersion data of the intact virus and those of the protein rods, a "calculated" rotatory dispersion curve of the RNA in the virus has been obtained. This rotatory dispersion curve is different from that obtained with the isolated RNA, both of which show Cotton effects in the ultraviolet region. From the fact that the inflection point of the rotatory dispersion curve of the isolated RNA in concentrated urea solution approximates that of the "calculated" dispersion curve, it is concluded that there is no interaction between bases of the RNA in the native TMV.

We are pleased to acknowledge several interesting discussions with Drs. D. L. D. Caspar and Carolyn Cohen.

REFERENCES

1. KLUG, A., and CASPAR, D. L. D., *Advances in Virus Research*, **8**, in press.
2. FRAENKEL-CONRAT, H., *Virology*, 1957, **4**, 1.
3. SCHRAMM, G., and ZILLIG, W., *Z. Naturforsch.*, 1955, **10 b**, 493.
4. FRANKLIN, R. E., *Biochim. et Biophysica Acta*, 1955, **18**, 313; *Nature*, 1956, **177**, 929.
5. FRANKLIN, R. E., CASPAR, D. L. D., and KLUG, A., *in* Plant Pathology: Problems and Progress, 1908-1958, (C. S. Holton, editor), Madison, University of Wisconsin Press, 1959, 447.
6. GIERER, A., *Nature*, 1957, **179**, 1297; *Z. Naturforsch.*, 1958, **13 G**, 477.
7. BOEDTKER, H., *Biochim. et Biophysica Acta*, 1959, **32**, 519.
8. ANDERER, F. A., UHLIG, H., WEBER, E., and SCHRAMM, G., *Nature*, 1960, **186**, 922.
9. FRASER, R. D. B., *Nature*, 1952, **170**, 491.
10. BEERS, M., *Biochim. et Biophysica Acta*, 1958, **29**, 423.
11. Kindly supplied by Professor S. G. Wildman, Department of Plant Pathology, University of California, Los Angeles.
12. SIEGEL, A., and WILDMAN, S. G., *Phytopathology*, 1954, **44**, 277.
13. HOLMES, K. G., and CASPAR, D. L. D., personal communication.
14. COHEN, S., and STANLEY, W. M., *J. Biol. Chem.*, 1942, **144**, 589.
15. (*a*) MOFFITT, W., *J. Chem. Physics*, 1956, **25**, 467. (*b*) MOFFITT, W., *Proc. Nat. Acad. Sc.*, 1956, **42**, 736. (*c*) MOFFITT, W., FITTS, D. D., and KIRKWOOD, J. C., *Proc. Nat. Acad. Sc.*, 1957, **43**, 723.
16. For original references see Blout, E. R., Polypeptides and proteins, *in* Optical Rotatory Dispersion, (C. Djerassi, editor), New York, McGraw-Hill Book Company, 1960, 238.
17. SIMMONS, N. S., COHEN, C., SZENT-GYORGYI, A. G., WETLAUFER, D. B., and BLOUT, E. R., data to be published.
18. BLOUT, E. R., DE LOZÉ, C., BLOOM, S. M., and FASMAN, G. D., *J. Am. Chem. Soc.*, 1960, **82**, 3787.
19. FASMAN, G. D., and BLOUT, E. R., data to be published.
20. MCRAE, E. G., and KASHA, M., *J. Chem. Physics*, 1958, **28**, 721.

CHANGES IN QUANTUM YIELD OF PHOTOSYNTHESIS IN THE RED ALGA *Porphyridium cruentum* CAUSED BY STEPWISE REDUCTION IN THE INTENSITY OF LIGHT PREFERENTIALLY ABSORBED BY THE PHYCOBILINS

J. B. THOMAS *and* GOVINDJEE

From the Photosynthesis Research Laboratory, Botany Department, University of Illinois, Urbana. Dr. Thomas' present address is Biophysical Research Group, Physical Institute of the State University, Utrecht, the Netherlands

ABSTRACT This paper describes the relation between the quantum yield of photosynthesis in the red alga *Porphyridium cruentum*, and the spectral composition of light, changed by filtering white light through aqueous phycobilin solutions of increasing optical density. At sufficiently high densities of the filter solution, no measurable photosynthesis can be observed, although chlorophyll *a* molecules are still being excited at a significant rate, as can be proved by calculations from spectral distribution curves, and is confirmed by the occurrence of a "second Emerson effect" upon addition of orange light. An interpretation of this result, based on other experiments, will be given in a subsequent paper. A modification of the opal glass technique for reducing the effect of scattering when measuring absorption, was developed in connection with this research, and also is described in the paper.

INTRODUCTION

In the red region, the quantum yield of photosynthesis drops with increasing wavelength of the actinic light (*cf.* Emerson and Lewis (6); Haxo and Blinks (17)). Emerson and coworkers (1, 4, 8-11) found that this low quantum yield can be raised to approximately normal values by exciting, in addition to chlorophyll *a*, one or more of the auxiliary pigments. This phenomenon, known as the "second Emerson effect," has been interpreted by Emerson as evidence of a need for cooperation between the excited molecules of an auxiliary pigment and those of chlorophyll *a*. Ef-

This research was supported by National Science Foundation research grant G4969.
Received for publication, June 3, 1960.

fective auxiliary pigments include chlorophyll *b*, phycobilins, and, among the carotenoids, at least fucoxanthol (*cf.* Emerson and Rabinowitch (11)).

According to Govindjee and Rabinowitch (15), light absorption in one of the chlorophyll *a* forms *in vivo*—the form which has an absorption peak at 670 mμ (chl *a* 670)—can complement, in green and brown algae, the light absorption above 680 mμ as effectively as light absorption in chlorophyll *b*. This suggests that what is really needed for high quantum yield of photosynthesis, is balanced excitation of two forms of chlorophyll *a*. In other words, chl *a* 670 acts as an "auxiliary pigment" to some other chlorophyll *a* form (or forms) (chl *a* 680 or chl *a* 690). Absorption above 680 mμ leads (in green algae) mainly or exclusively to one type of excitation, and therefore to a low quantum yield; the other type of excitation can be obtained either directly, by absorption in chl *a* 670, or indirectly, by energy transfer from an auxiliary pigment to chl *a* 670.

According to Emerson and Chalmers (10), the extent of short wave stimulation of the quantum yield in far red light depends on the intensity ratio between the "short-wave light" and the "long-wave light." This ratio must exceed a certain minimum value in order to produce any effect at all.

As to the nature of the two types of excitation, Franck (5, 12), suggested (*a*) excitation to the metastable triplet state, and (*b*) excitation to the fluorescent singlet state. Which excited state is obtained, depends on whether the chlorophyll molecules find themselves in a hydrophilic medium, in which case the primary excited fluorescent singlet state lives long enough to contribute to the photochemical process, or in a lipophilic medium, in which case the fluorescent state is converted practically instantaneously into the triplet state.

Another alternative was suggested by Lavorel (18) and S. Brody (2); namely, that the two types of excitations are those of chlorophyll *a* in the monomeric state and in the dimeric state, respectively. The first excited state is fluorescent, and the second non-fluorescent (probably because of immediate conversion into the metastable triplet state).

Emerson's measurements (6) were not extended far enough into the infrared to decide whether the yield of photosynthesis in the far red wing of the chlorophyll *a* absorption band declines to zero, or to a finite low value. These measurements ended at 700 mμ, where the quantum yield had a value of about 0.01; while chlorophyll *a* absorbs, *in vivo*, up to about 720 mμ. If the quantum yield could be reduced to zero while the absorption by chlorophyll *a* still remained finite, one could conclude that chlorophyll *a* (or, at least, the form of chlorophyll *a* responsible for absorption in the far red wing of the absorption band) is, in itself, entirely incapable of photosynthesis.

We tried to approach this problem by illuminating algae with white light, from which the wavelengths preferentially absorbed by the auxiliary pigments could be gradually removed. The red alga *Porphyridium cruentum* was chosen as object. Since red algae contain no chlorophyll *b*, the absorption bands of their major aux-

iliary pigments, the phycobilins, are well separated from those of chlorophyll *a*. It is therefore possible to vary the ratio of the amount of light absorbed by the auxiliary pigments to that absorbed by chlorophyll *a* by small increments over a wide range, with the help of light filters consisting of phycobilin extracts of increasing concentration. The results of this study are described below. For a preliminary note, see (21).

MATERIALS AND METHODS

Preparation of Algae. *Porphyridium cruentum* was grown in the medium described by M. Brody and Emerson (3) at about 22°C over ten 15 watt flourescent light tubes located about 15 cm below the bottom of the flasks. An inoculum of about 100 μl of cells in 200 ml of the medium, contained in 300 ml culturing flasks, was used. Air containing 5 per cent carbon dioxide was bubbled through the cultures, which were continuously shaken. In order to reduce respiration, the light intensity was decreased during the last 2 days previous to the experiment, by using only two out of the ten fluorescent tubes. After 6 or 7 days of culturing, the cells were harvested by centrifugation and washed twice in Warburg buffer No. 11, with NaCl added in the following proportion: 16 gm $NaHCO_3$ + 1 gm Na_2CO_3 + 15.2 gm NaCl, in 1 liter of glass-distilled water. The suspension was diluted by the same medium, to a concentration giving about 30 per cent absorption of white light in 1 cm path.

Preparation of Phycobilins for Filters. Large amounts of aqueous phycobilin extracts were prepared from *Porphyra perforata*.[1] The fronds were rinsed with tap water, washed, and stored in distilled water, at room temperature in the dark for 5 or more days. The cells died during this period, and released the major part of the phycobilins, but no chlorophyll or carotenoids. By decanting this extract, washing the algae with distilled water once more, and storing them under the same conditions for 5 more days, an extract of phycoerythrin free from phycocyanin could be obtained.

The extracts were filtered through a Seitz filter, using filter sheets No. 3. Next, following Fujiwara (14), the phycobilins were precipitated by adding a solution containing 44 weight per cent of reagent-grade ammonium sulfate. After filtration, the precipitates were washed with the same ammonium sulfate solution and redissolved in glass-distilled water. In this way, highly concentrated pigment solutions could be obtained. They were dialyzed against glass-distilled water for at least 12 hours. Some grayish white precipitation was formed, and removed by centrifugation. The clear, intensely colored solutions were stored in a refrigerator. Upon standing, more grayish white precipitate was formed. Therefore, the pigment solution was recentrifuged before each experiment. In light, the extracted pigments showed some bleaching. Hence, optical density had to be checked before each experiment.

Phycocyanin extracts were prepared from the blue-green alga *Anacystis nidulans* by supersonic treatment and subsequent removal of chlorophyll by fractional precipitation with ammonium sulfate. They were stored in the refrigerator and repeatedly checked for absorption changes.

Calibration of Filters. The required densities of the "phycobilin filter" were obtained either by diluting the original preparation, or by using several cuvettes containing undiluted solution. The filters were placed in the actinic white light beams. For

[1] Our thanks are due to Dr. L. R. Blinks for kindly providing us with these algae.

practical reasons, zero order light passed through the Emerson grating monochromator was used. A 225 watt ribbon filament lamp served as light source. If necessary, the light intensity could be reduced by wire screens. Care was taken to weaken the non-absorbable infrared radiation by using a 6 inch water filter together with two American Optical Company heat-absorbing glass filters; an approximate correction was applied for the residual amount of radiation beyond 720 mμ. This correction was determined by plotting the product of the emission curve of the lamp and of the transmission curve of the filters, and computing the area of the graph at wavelengths exceeding 720 mμ in per cent of the total area from 400 to 2000 mμ. For white light, the correction was 37 per cent. A similar factor was determined also for light transmitted by each of the phycobilin filters used. Orange "background light" could be supplied by a 1000 watt air-cooled lighthouse incandescent lamp, run at about 700 watts and provided with two heat-absorbing filters in

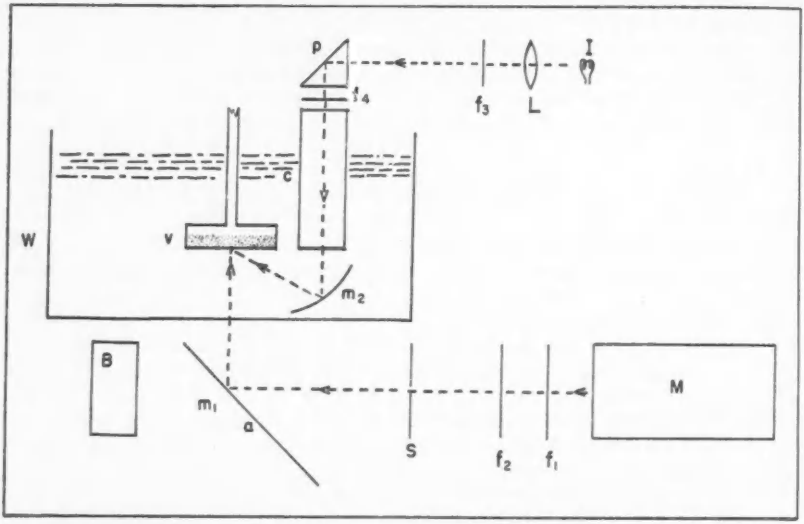

FIGURE 1 Scheme of the optical system. *M*, monochromator; f_1 and f_3, *infrared*-absorbing filters; f_2, "phycobilin filter"; f_4, orange filter; *S*, exit slit; m_1, glass mirror, movable around axis *a*; *B*, bolometer; *W*, water bath; *v*, vessel with algal suspension; m_2, stainless steel mirror; *c*, lucite column; *p*, reflecting prism; *L*, lens, *I*, lamp.

addition to a 3 mm thick Corning glass filter No. 3480. A diagram of the arrangement is shown in Fig. 1. Light energy was measured with a bolometer as described by Emerson and Chalmers (7). True (*i.e.*, scattering-free) light absorption of the algal suspension in white light, as well as in light transmitted by the phycobilin filters, was determined in an integrating sphere instrument, built by Mr. C. Cederstrand in our laboratory, which will be described in a separate paper.

Measurement of Oxygen Liberation. Photosynthetic oxygen evolution was measured in the differential manometer described by Emerson and Chalmers (7). The experimental vessel contained 7 ml of cell suspension. The temperature was 10°C. Readings were made every minute. As a rule, each measuring period included 8 readings; the first 3

were discarded and a mean value was computed from the next 5. If the readings were not stationary after a 3 minutes' adjustment period, this period was extended until the measurements were constant, and the 5 subsequent readings were used. At least 4 such sets of measurements were made in each case (2 in darkness, alternating with 2 in light) to calculate the light action. Mean errors were computed according to the formula:

$$\text{M.E.} = \sqrt{\frac{\Sigma d^2}{n(n-1)}}$$

Determination of Absorption Spectra. A modification of the opal glass or oiled filter paper technique of Shibata *et al.* (19), was developed to measure the absorption spectrum of algal suspensions. Whatman filter paper No. 1 was cut into strips which just fitted into 1 cm wide Beckman absorption cuvettes. One strip was soaked in a dense

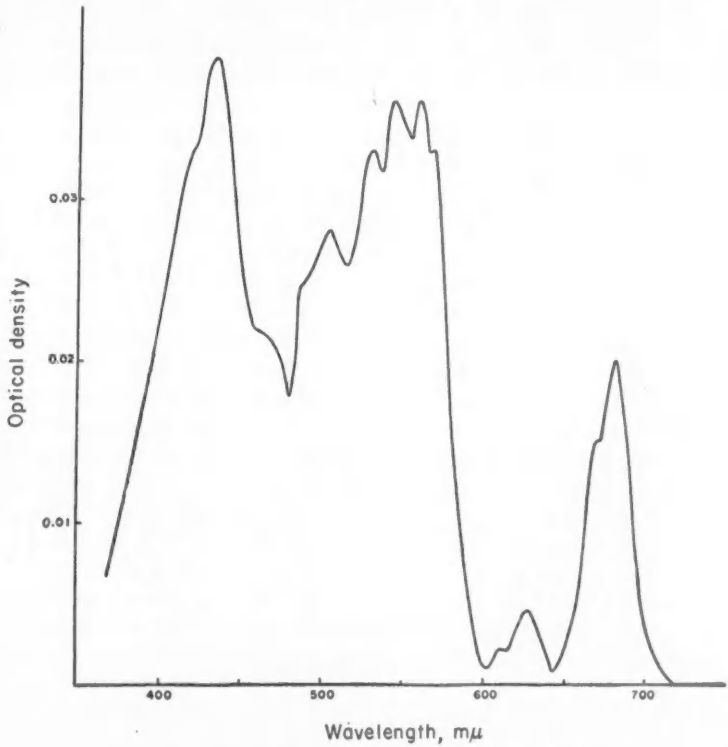

FIGURE 2 Absorption spectrum of *Porphyridium cruentum*.

cell suspension and adjusted to the inner side of the wall of the empty cuvette facing the phototube. One or two drops of the suspension were added at the bottom of the cuvette in order to prevent evaporation. Then, the cell was closed. The meniscus of the liquid

layer was well below the light beam. A cuvette containing a similar paper strip soaked with distilled water (or culture medium) was used as a blank. The scattering by the filter paper strips varied slightly. Since measurements in the integrating sphere showed that the absorption of *Porphyridium* is zero at 800 mμ, all experimental curves were shifted, up or down, so as to make the absorption value at 800 mμ equal to zero. This served as an approximate correction for variations in the scattering power of filter strips. Clearly, this method cannot be used for quantitative purposes; but it enables detailed spectral characterization with only a few drops of a highly scattering suspension (*cf.* Fig. 2).

RESULTS AND DISCUSSION

Absorption Spectrum of Porphyridium cruentum. The absorption spectrum of a sample culture of *Porphyridium cruentum*, obtained in the above described manner, is shown in Fig. 2. As evident from the absorption around 625 mμ,

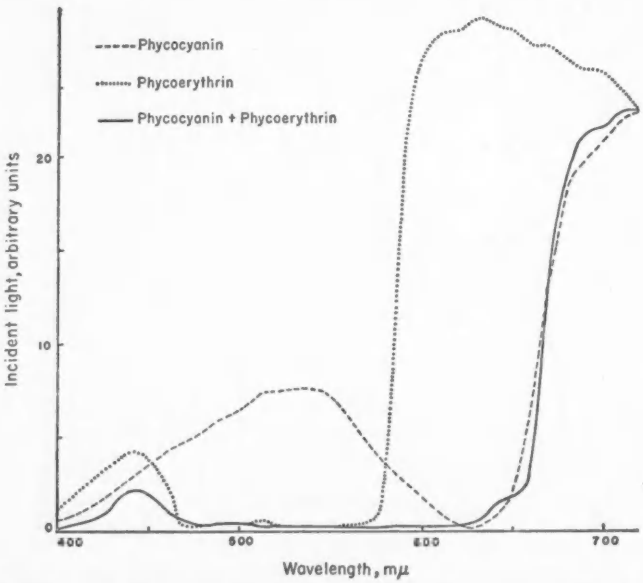

FIGURE 3 Composition of actinic light after passing an aqueous solution of phycocyanin from *Anacystis nidulans*, a solution of phycoerythrin from *Porphyra perforata*, and a mixture of both phycobilins from the latter species.

Porphyridium cruentum contains only a very small amount of phycocyanin. (Part of the absorption in this region is due to a minor band of chlorophyll *a*.)

A distinct shoulder can be noted in Fig. 2 on the short wave side of the main

chlorophyll *a* band. In this case, the shoulder and the main maximum are at 670 and 682 mμ, respectively; in other cultures, their locations varied between 670 and 674 mμ for the first, and 678 and 682 mμ for the second. The occurrence of such a shoulder in the red absorption band of chlorophyll *a in vivo* has also been noted and discussed by Halldal (16), French and Young (13), and Thomas and Marsman (20). Leaving aside specific interpretation of the two forms of chlorophyll *a in vivo,* which must be postulated to account for the two bands, we will designate them, regardless of the exact location of the absorption bands, as chl *a* 670 and chl *a* 680, respectively.

Transmission Characterization of the Filters. Fig. 3 shows the composition of the light transmitted by "phycobilin filters" of the highest density used. The product of the emission curve of the lamp and the per cent transmission curve of a filter was plotted for this purpose *versus* wavelength. With the phycoerythrin filter, the incident light consists mainly of wavelengths longer than 580 mμ, and of a weak band around 440 mμ. With the phycocyanin filter, this light is composed of wavelengths longer than about 650 mμ, plus a broad band with a maximum at 520 to 540 mμ, in the region where phycoerythrin absorbs most strongly. With both phycobilins, the incident light consists nearly exclusively of wavelengths longer than about 660 mμ. If the energy of distribution of the latter is multiplied by the absorption coefficient of chlorophyll *a* in *Porphyridium,* (*cf.* Fig. 4), it becomes evident that chl *a* 680 is excited by this light much more efficiently than chl *a* 670.

Quantum Yield in Relation to Filter Density. Fig. 5 shows the results of six experiments on the relation between the per cent light transmission by "mixed phycobilin" filters of various optical densities, and the quantum yield of photosynthesis, expressed in per cent of that in white light. The plotted mean values are obtained by averaging the results of six single experiments. The vertical lines show the range of variations of the individual results. Since differences in photosynthetic activity of the studied cultures are coresponsible for this scattering of results, the errors are, as a rule, higher than those calculated for each single experiment. For pressure changes of 10 μl/hour or more, the variation did not exceed 3 per cent.

It is apparent from Fig. 5 that the relationship between the quantum yield and the percentage of white light transmitted by the phycobilin filters of various densities cannot be described by a single linear function. As the transmission is decreased from 100 to 80 per cent, ϕ does not change. Reducing the transmission further, a linear decrease of ϕ occurs until the light intensity is down to 20 per cent. If the density of the filter is increased still further, the rate of decline of ϕ is accelerated, until the quantum yield is practically zero at a filter density still allowing about 5 per cent of the light to pass.

The nature of the relationship shown in the graph may be explained qualitatively in terms of the dependence of the quantum yield on the intensity ratio of the auxiliary light and of the far red light, noted by Emerson and Chalmers (10). When using

phycobilin filters transmitting 100 to 80 per cent, the proportion of the light absorbed by the phycobilins in the algal cells, may be high enough to make this ratio exceed the critical value suggested by Emerson's results. Further reducing this proportion by applying filters with 80 to 20 per cent transmission causes ϕ to decline linearly with decreasing filter transmission. When, by using filters of a still higher density, a certain minimal value of this ratio is passed, the auxiliary light becomes unable to produce any effect, and the yield drops sharply. Depending on whether light absorbed exclusively by chlorophyll *a* (or a certain form of chlorophyll *a*) does or does not produce photosynthesis with a finite quantum yield, ϕ should drop to a certain small but constant value, or decline to zero. Fig. 5 suggests that the latter may be true. Using a mixed phycobilin filter absorbing 95 per cent of incident

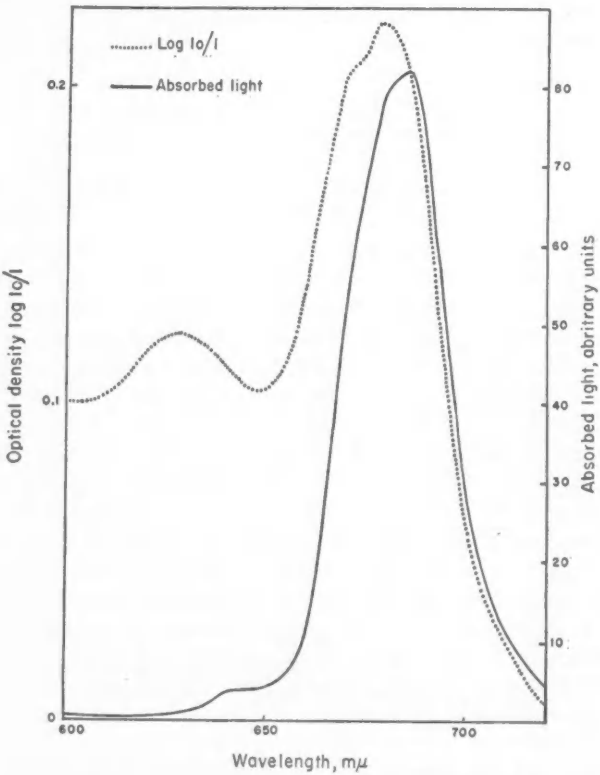

FIGURE 4 Absorption curve of chlorophyll *a* in the living cell, and composition of light absorbed by chlorophyll from light filtered through densest filter of mixed phycobilins.

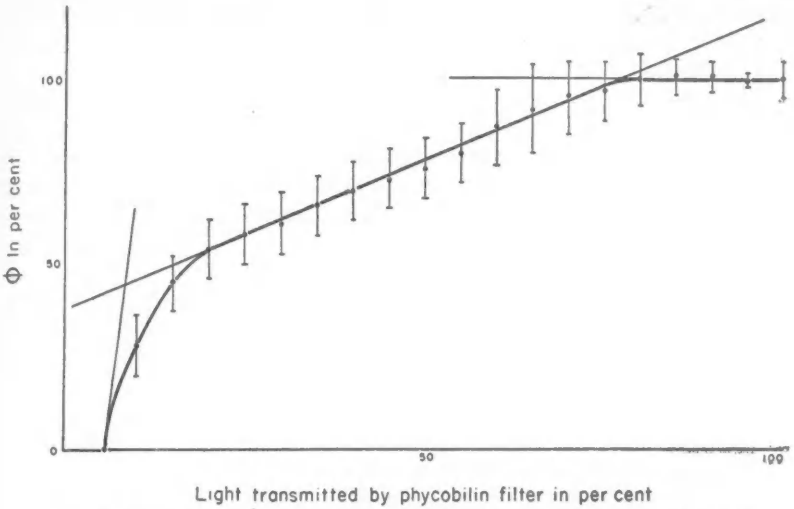

FIGURE 5 Relation between the proportion of incident white light transmitted by mixed phycobilin filters of various optical densities, and the relative quantum yield.

white light (referred to below as PB-95), no photosynthetic activity could be measured at all. The intensity incident on the vessel still amounted to 2 to 4 μeinsteins/hour, and chlorophyll *a* was markedly excited by the incident light. This is strikingly demonstrated by the occurrence of the Emerson effect, shown in Table I. Without orange background light, photosynthetic oxygen evolution was below the measuring range. When orange light was added, a measurable rate of oxygen production had to be attributed to light transmited by PB-95.

Two additional experiments were made in which, instead of the PB-95 filter,

TABLE I

EMERSON EFFECT ON PHOTOSYNTHETICALLY INACTIVE LIGHT TRANSMITTED BY A PB-95 FILTER

Experiment No.	Oxygen evolution attributable to light transmitted by PB-95	
	Without background light	With orange background light
	μl/hr.	μl/hr.
a	−0.60	+1.20
b	−0.60	+2.40
c	0.00	+2.40
d	+0.53	+1.14
e	−0.54	+1.17
Mean	−0.24 ± 0.25	+1.66 ± 0.30

either a phycocyanin or a phycoerythrin filter of comparable optical density at the absorption maxima was used. In these experiments, photosynthesis was clearly measurable—obviously due to transmission of some short wave light.

The conclusion which one could be inclined to draw from these results, that in the studied organism, chlorophyll *a* (or the form of chlorophyll *a* absorbing above 680 mμ) is by itself unable to produce photosynthesis, contradicts the observation of M. Brody and Emerson (4) (confirmed by us) that photosynthesis does occur when the same algae are irradiated with narrow spectral bands, up to 700 mμ. This disagreement will be discussed in a succeeding paper.

We are grateful to Professor E. Rabinowitch for stimulating discussion. We owe thanks for assistance to Mrs. Rajni Govindjee and Mrs. Judith Twarog, and to Mr. C. Cederstrand for his help in performing absorption measurements.

REFERENCES

1. BRODY, M., 1958, Thesis, University of Illinois, Urbana, Illinois.
2. BRODY, S., 1958, *Science*, **128**, 838.
3. BRODY, M., and EMERSON, R., 1959, *Am. J. Bot.*, **46**, 433.
4. BRODY, M., and EMERSON, R., 1959, *J. Gen. Physiol.*, **43**, 251.
5. BRUGGER, J. E., and FRANCK, J., 1958, *Arch. Biochem. and Biophysics*, **75**, 415.
6. EMERSON, R., and LEWIS, C. M., 1943, *Am. J. Bot.*, **30**, 165.
7. EMERSON, R., and CHALMERS, R., 1955, *Plant Physiol.*, **30**, 504.
8. EMERSON, R., CHALMERS, R., CEDERSTRAND, C., and BRODY, M., 1956, *Science*, **123**, 673.
9. EMERSON, R., CHALMERS, R., and CEDERSTRAND, C., 1957, *Proc. Nat. Acad. Sc.*, **43**, 133.
10. EMERSON, R., and CHALMERS, R., 1958, *Phycol. Soc. Am. News Bull.*, **11**, 51.
11. EMERSON, R., and RABINOWITCH, E., 1960, *Plant Physiol.*, **35**, 477.
12. FRANCK, J., 1958, *Proc. Nat. Acad. Sc.*, **44**, 941.
13. FRENCH, C. S., and YOUNG, V. M. K., 1956, *in* Radiation Biology, (A. Hollaender, editor), New York, McGraw-Hill Book Co., **3**, 343.
14. FUJIWARA, T., 1955, *J. Biochem.*, **42**, 411.
15. GOVINDJEE, and RABINOWITCH, E., 1960, *Science*, **132**, 355.
16. HALLDAL, P., 1958, *Physiol. Plantarum*, **11**, 401.
17. HAXO, F., and BLINKS, L. R., 1950, *J. Gen. Physiol.*, **33**, 389.
18. LAVOREL, J., 1957, *J. Physic. Chem.*, **61**, 1600.
19. SHIBATA, K., BENSON, A. A., and CALVIN, M., 1954, *Biochim. et Biophysica Acta*, **15**, 461.
20. THOMAS, J. B., and MARSMAN, J. W., 1959, *Biochim. et Biophysica Acta*, **35**, 316.
21. THOMAS, J. B., and GOVINDJEE, 1960, Paper presented to the Conference on Light and Life, McCollum-Pratt Institute, Baltimore.

LETTERS TO THE EDITOR

Brief letters to the Editor that make specific scientific reference to papers published previously in the BIOPHYSICAL JOURNAL *are invited. Receipt of such letters will not be acknowledged but those containing pertinent scientific comments and scientific criticisms will be published.*

ANNOUNCEMENTS

International Congress of Biophysics

An International Congress of Biophysics will be held in Stockholm from July 31 to August 4, 1961. The purpose of the meeting is to provide a forum for international communication in the field of biophysics. Participants may include members of national societies of biophysics, medical physics, and related fields; and other scientists interested in pure and applied biophysics. The meeting will be divided between a series of symposia devoted to special topics in biophysics and to presentations of a number of contributed papers in pure and applied biophysics submitted by the participants. Further information can be obtained from Dr. Bo Lindström at the Department of Medical Physics, Karolinska Institutet, Stockholm 60, Sweden.

International Symposium on the Transmission and Processing of Information

The Professional Group on Information Theory of the Institute of Radio Engineers, in cooperation with the Center of Communication Sciences, Research Laboratory of Electronics, Massachusetts Institute of Technology, is planning to hold an International Symposium on the Transmission and Processing of Information on September 6 to 8, 1961. This Symposium will be held at the Massachusetts Institute of Technology, Cambridge, Massachusetts.

The purpose of the Symposium will be to provide an outstanding occasion for the presentation of significant new research contributions, of either a theoretical or experimental nature. As in the case of the similar 1954 and 1956 symposia, no tutorial papers will appear; the program will be planned specifically for active specialists in the field. In order to provide opportunity for creative and thorough discussion, the Symposium TRANSACTIONS will be distributed at least two weeks prior to the meetings.

Submission of papers is hereby invited. In order to carry out the publication plans successfully, the following deadline schedule is necessary.

Receipt of 500-1000 word Abstracts: January 1, 1961
Receipt of full-length Papers: April 1, 1961

Authors will be notified of the preliminary acceptance of their Abstracts by January 20; the final program selection will be made on the basis of the complete Papers, and authors notified by May 1. Abstracts and Papers should be submitted to the Chairman of the Organizing Committee, R. M. Fano, Research Laboratory of Electronics, Massachusetts Institute of Technology, Cambridge 39, Massachusetts.

Announcements of direct interest to the Biophysical Society will be acceptable. Receipt of announcements will not be acknowledged but appropriate ones will be printed. Conciseness and clarity are factors in the decision to print an announcement.